J|A|C|S
ARTICLES
Published on Web 11/08/2006

Conformationally Constrained 2′-*N*,4′-*C*-Ethylene-Bridged Thymidine (Aza-ENA-T): Synthesis, Structure, Physical, and Biochemical Studies of Aza-ENA-T-Modified Oligonucleotides

Oommen P. Varghese, Jharna Barman, Wimal Pathmasiri, Oleksandr Plashkevych, Dmytro Honcharenko, and Jyoti Chattopadhyaya*

Contribution from the Department of Bioorganic Chemistry, Box 581, Biomedical Center, Uppsala University, SE-75123 Uppsala, Sweden

Received May 25, 2006; E-mail: jyoti@boc.uu.se

Abstract: The 2′-deoxy-2′-*N*,4′-*C*-ethylene-bridged thymidine (aza-ENA-T) has been synthesized using a key cyclization step involving 2′-*ara*-trifluoromethylsufonyl-4′-cyanomethylene **11** to give a pair of 3′,5′-*bis*-OBn-protected diastereomerically pure aza-ENA-Ts (**12a** and **12b**) with the fused piperidino skeleton in the chair conformation, whereas the pentofuranosyl moiety is locked in the North-type conformation ($7° < P < 27°$, $44° < \phi_m < 52°$). The origin of the chirality of two diastereomerically pure aza-ENA-Ts was found to be due to the endocyclic chiral 2′-nitrogen, which has axial N−H in **12b** and equatorial N−H in **12a**. The latter is thermodynamically preferred, while the former is kinetically preferred with $E_a = 25.4$ kcal mol^{-1}, which is thus far the highest observed inversion barrier at pyramidal N−H in the bicyclic amines. The 5′-*O*-DMTr-aza-ENA-T-3′-phosphoramidite was employed for solid-phase synthesis to give four different singly modified 15-mer antisense oligonucleotides (AONs). Their AON/RNA duplexes showed a T_m increase of 2.5−4 °C per modification, depending upon the modification site in the AON. The relative rates of the RNase H1 cleavage of the aza-ENA-T-modified AON/RNA heteroduplexes were very comparable to that of the native counterpart, but the RNA cleavage sites of the modified AON/RNA were found to be very different. The aza-ENA-T modifications also made the AONs very resistant to 3′ degradation (stable over 48 h) in the blood serum compared to the unmodified AON (fully degraded in 4 h). Thus, the aza-ENA-T modification in the AON fulfilled three important antisense criteria, compared to the native: (i) improved RNA target affinity, (ii) comparable RNase H cleavage rate, and (iii) higher blood serum stability.

Introduction

Modified oligonucleotides have successfully been used as valuable tools to inhibit gene expression by utilizing various mechanisms of action.[1−7] The most matured method is the antisense technology,[6,8] which exploits the ability of a single-stranded DNA oligonucleotide to bind to the target messenger RNA (mRNA) via Watson−Crick base pairing in a sequence-specific manner. Once bound to the target RNA, the antisense agent either sterically blocks the synthesis of ribosomal proteins or induces RNase-H-mediated degradation of the target mRNA. The modified oligonucleotides have also been found useful as short double-stranded RNA (siRNA),[7,9−11] which silence gene expression utilizing a naturally occurring mechanism called RNA interference (RNAi).

For *in vivo* applications[12,13] of the oligonucleotide-based approaches, appropriate chemical modifications[14,15] are warranted to enhance target affinity, specificity, and stability toward the endo- and exonucleases, as well as tissue-specific delivery to improve the overall pharmacokinetic properties. It is a challenge to come up with optimally modified monomer blocks with a natural phosphate backbone that can successfully address all of the above issues related to the improvement of the pharmacokinetic properties.[14,16]

Among various sugar, phosphate, and nucleobase modifications reported,[14,15] synthetic oligonucleotides having conformationally constrained furanose-fused bi- and tricyclic carbohydrate moieties[17−31] (Figure S1 and Discussion S1 in the Supporting Information) or a modified pyranose derivative[16,32,33] in the

(1) Helene, C. *Eur. J. Cancer* **1991**, *27*, 1466.
(2) Vasquez, K. M.; Wilson, J. *Trends Biochem. Sci.* **1998**, *23*, 4.
(3) Chech, T. R.; Zaug, A. J.; Grabowski, P. J. *Cell* **1981**, *27*, 487.
(4) Kruger, K.; Grabowski, P. J.; Zaug, A. J.; Sands, J.; Gottschling, D. E.; Chech, T. R. *Cell* **1982**, *31*, 147.
(5) Schubert, S.; Gül, D. C.; Grunert, H. P.; Grunert, H.; Erdmann, V. A.; Kurreck, J. *Nucl. Acids Res.* **2003**, *31*, 5982.
(6) Crooke, S. T. *Annu. Rev. Med.* **2004**, *55*, 61.
(7) Fire, A.; Xu, S.; Motegomery, M. K.; Kostas, S. A.; Driver, S. E.; Mello, C. C. *Nature* **1998**, *391*, 806.
(8) Brenda, F. B.; Brett, P. M. *Biochem. Biophys. Acta* **1999**, *1489*, 3.
(9) Hutvagner, G.; Zamore, P. D. *Science* **2002**, *297*, 2056.
(10) Novina, C. D.; Sharp, P. A. *Nature* **2004**, *430*, 161.
(11) Xia, J.; Noronha, A.; Toudjarska, I.; Li, F.; Akinc, A.; Braich, R.; Frank-Kamenetsky, M.; Rajeev, G. K.; Egli, M.; Manoharan, M. *Chem. Biol.* **2006**, *1*, 176.
(12) Stephenson, M. L.; Zamecnik, P. C. *Proc. Natl. Acad. Sci. U.S.A.* **1978**, *75*, 285.
(13) Zamecnik, P. C.; Stephenson, M. L. *Proc. Natl. Acad. Sci. U.S.A.* **1978**, *75*, 280.
(14) Kurreck, J. *Eur. J. Biochem.* **2003**, *270*, 1628.
(15) Freier, S. M.; Altmann, K. H. *Nucleic Acids Res.* **1997**, *25*, 4429.
(16) Herdewijn, P. *Biochim. Biophys. Acta* **1999**, *1489*, 167.
(17) Wengel, J. *Acc. Chem. Res* **1999**, *32*, 301.
(18) Steffens, R.; Leumann, C. J. *J. Am. Chem. Soc.* **1997**, *119*, 11548.
(19) Meldgaard, M.; Wengel, J. *J. Chem. Soc., Perkin Trans. 1* **2000**, 3539.
(20) Leumann, C. J. *Bioorg. Med. Chem.* **2002**, *10*, 841.

monomer nucleotide units have been found to be promising in terms of target RNA binding, accessibility, and nuclease resistance. The enhanced target-binding ability of oligonucleotides modified with North-conformationally constrained sugar units[23,34−40] can be attributed to the conformational preorganization by improved stacking between the nearest neighbors,[41] thereby minimizing the entropic energy penalty in the free energy of stabilization for the duplex formation with RNA.

Koizumi et al.[42] have shown that the 2′-*O*,4′-*C*-ethylene-bridged nucleoside[22,42] (ENA) (structure **I** in Figure S1 in the Supporting Information) modified antisense oligonucleotides (AONs) have approximately 55 times higher stability toward 3′-exonuclease compared to the locked nucleic acid (LNA) analogue.[37] The ability of ENA for efficient target binding and high nuclease resistance has been well-exploited to evaluate its antisense,[37,43−46] antigene,[47] and RNAi[37,45−48] properties.

The ENA-modified AONs have been shown to have unique properties, such as high target RNA affinity (+3.5 to +5.2 °C per modification),[42] sequence selectivity toward ssRNA/dsDNA targets,[47] and high nuclease resistance (*in vivo* and *in vitro*),[22,37,46] *in vivo* RNase recruitment,[37] and triplex forming[47] properties. This prompted us to design and synthesize the conformationally constrained 2′-*N*,4′-*C*-ethylene-bridged ENA-thymidine (aza-ENA-T, structure **F** in Scheme 1) and incorporate it into the AONs to explore their potential for effective gene-directed therapeutics and diagnostics. The aza-ENA-based AONs may have three clear advantages over the corresponding ENA-containing counterparts in a similar manner as the 2′-amino-LNA-modified AONs have over the LNA-modified counterparts.[25,49] First, the endocyclic amino functionality of the aza-ENA analogue could be utilized as a well-defined conjugation site,[50] and thereby, we can control the hydrophilic, hydrophobic, and steric requirements of a minor groove of the duplex. Second, the amine-derivatized AONs have displayed increased thermal affinities[51,52] toward complementary RNA, possibly because of the presence of positively charged moieties at physiological pH, and thus could influence partial neutralization of the negatively charged phosphates in the duplexes.[25,31,53] Third, introduction of a fluorescence probe connected to this nitrogen moiety will enable us for real-time *in vivo* imaging of RNA and can therefore be used for specific detection of nucleic acids while maintaining their hybridization properties.[49,54]

We report here synthesis of aza-ENA-T, physicochemical, nuclear magnetic resonance (NMR), and computational structural studies of aza-ENA-T and biochemical studies of aza-ENA-T containing oligonucleotides. The NMR and computational structural studies of aza-ENA-T showed that the *piperidino* moiety of the aza-ENA-T is indeed locked in the chair conformation (with the nitrogen lone pair in the axial position and the N−H proton in the equatorial position), whereas the fused sugar is constrained to a North-type conformation similar to that of the 2′-*O*,4′-*C*-ethylene-bridged ENA analogue.[22,42] Finally, the aza-ENA-T nucleotides have been incorporated in 15-mer AONs as a single modification at four different sites to give four mono-aza-ENA-T-substituted AONs 2−5 (sequences shown in Table 1). These AON/RNA duplexes have shown an increase in the thermal stability by +2.5 to +4 °C per modification toward complementary RNA, depending upon the substitution site. We also show that the relative rates of the RNase-H1-promoted cleavage of the aza-ENA-T-modified AON/RNA heteroduplexes are comparable to that of the native counterpart, and quite interestingly, the aza-ENA-T modifications also result in a significant increase of the AON resistance to 3′-exonuclease degradation in the blood serum compared to the native counterpart. No blood serum stability or the RNase H recruitment capability study has thus far been reported for the 2′-amino-LNA-incorporated AONs, and hence, no direct comparison is yet possible with the aza-ENA-T-substituted AONs.

Results and Discussion

Synthesis of all 2′,4′-bridged nucleosides reported[21,22] thus far involve a nucleophilic displacement reaction with the nucleophile positioned at C2′ and a leaving group at the extended arm of C4′ (general structure "$\mathbf{A_1}$" in Scheme 1). We

(21) Koshkin, A. A.; Singh, S. K.; Nielson, P.; Rajwanshi, V. K.; Kumar, R.; Meldgaard, M.; Wengel, J. *Tetrahedron* **1998**, *54*, 3607.
(22) Morita, K.; Takagi, M.; Hasegawa, C.; Kaneko, M.; Tsutsumi, S.; Sone, J.; Ishikawa, T.; Imanishi, T.; Koizumi, M. *Bioorg. Med. Chem.* **2003**, *11*, 2211.
(23) Obika, S.; Nanbu, D.; Hari, Y.; Morio, K.-I.; In, Y.; Ishida, T.; Imanishi, T. *Tetrahedron Lett.* **1997**, *38*, 8735.
(24) Kumar, R.; Singh, S. K.; Koshkin, A. A.; Rajwanshi, V. K.; Meldgaard, M.; Wengel, J. *Bioorg. Med. Chem. Lett.* **1998**, *8*, 2219.
(25) Singh, S. K.; Kumar, R.; Wengel, J. *J. Org. Chem.* **1998**, *63*, 10035.
(26) Rajwanshi, V. K.; Hakansson, A. E.; Sorensen, M. D.; Pitsch, S.; Singh, S. K.; Kumar, R.; Nielsen, P.; Wengel, J. *Angew. Chem., Int. Ed.* **2000**, *39*, 1656.
(27) Sorensen, M. D.; Kvaerno, L.; Bryld, T.; Hakansson, A. E.; Verbeure, B.; Gaubert, G.; Herdewijn, P.; Wengel, J. *J. Am. Chem. Soc.* **2002**, *124*, 2164.
(28) Wang, G.; Gunic, E.; Girardet, J. L.; Stoisavljevic, V. *Bioorg. Med. Chem. Lett.* **1999**, *9*, 1147.
(29) Pradeepkumar, P. I.; Cheruku, P.; Plashkevych, O.; Acharya, P.; Gohil, S.; Chattopadhyaya, J. *J. Am. Chem. Soc.* **2004**, *126*, 11484.
(30) Pradeepkumar, P. I.; Chattopadhyaya, J. *J. Chem. Soc., Perkin Trans. 2* **2001**, 2074.
(31) Honcharenko, D.; Varghese, O. P.; Plashkevych, O.; Barman, J.; Chattopadhyaya, J. *J. Org. Chem.* **2006**, *71*, 299.
(32) Kozlov, I. A.; de Bouvere, B.; van Aerschot, A.; Herdewijn, P.; Orgel, L. E. *J. Am. Chem. Soc.* **1999**, *121*, 5856.
(33) Wang, J.; Verbeure, B.; Luyten, I.; Lescrinier, E.; Froeyen, M.; Hendrix, C.; Rosemeyer, H.; Seela, F.; van Aerschot, A.; Herdewijn, P. *J. Am. Chem. Soc.* **2000**, *122*, 8595.
(34) Tarkoy, M.; Bolli, M.; Schweizer, B.; Leumann, C. *Helv. Chim. Acta* **1993**, *76*, 481.
(35) Siddiqui, M. A.; Ford, H.; George, C.; Marquez, V. E. *Nucleosides Nucleotides* **1996**, *15*, 235.
(36) Wang, G.; Giradet, J. L.; Gunic, E. *Tetrahedron* **1999**, *55*, 7707.
(37) Morita, K.; Yamate, K.; Kurakata, S.; Abe, K.; Imanishi, T.; Koizumi, M. *Nucleic Acids Res. Sup.* **2002**, *2*, 99.
(38) Kvaerno, L.; Wengel, J. *J. Org. Chem.* **2001**, *66*, 5498.
(39) Babu, B. R.; Raunak; Poopeiko, N. E.; Juhl, M.; Bond, A. D.; Parmar, V. S.; Wengel, J. *Eur. J. Org. Chem.* **2005**, *11*, 2297.
(40) Kumar, T. S.; Madsen, A. S.; Wengel, J.; Hrdlicka, P. J. *J. Org. Chem.* **2006**, *71*, 4188−4201.
(41) Isaksson, J.; Acharya, S.; Barman, J.; Cheruku, P.; Chattopadhyaya, J. *Biochemistry* **2004**, *43*, 15996.
(42) Morita, K.; Hasegawa, C.; Kaneko, M.; Tsutsumi, S.; Sone, J.; Ishikawa, T.; Imanishi, T.; Koizumi, M. *Bioorg. Med. Chem. Lett.* **2002**, *12*, 73.
(43) Yagi, M.; Takeshima, Y.; Surono, A.; Takagi, M.; Koizumi, M.; Matsuo, M. *Oligonucleotides* **2004**, *14*, 33.
(44) Surono, A.; van Khanh, T.; Takeshima, Y.; Wada, H.; Yagi, M.; Takagi, M.; Koizumi, M.; Matsuo, M. *Hum. Gene Ther.* **2004**, *15*, 749.
(45) Morita, K.; Yamate, K.; Kurakata, S.-I.; Watanabe, K.; Imanishi, T.; Koizumi, M. *Nucleosides, Nucleotides Nucleic Acids* **2003**, *22*, 1619.
(46) Takagi, M.; Morita, K.; Nakai, D.; Nakagomi, R.; Tokui, T.; Koizumi, M. *Biochemistry* **2004**, *43*, 4501.
(47) Koizumi, M.; Morita, K.; Daigo, M.; Tsutsumi, S.; Abe, K.; Obika, S.; Imanishi, T. *Nucleic Acids Res.* **2003**, *31*, 3267.
(48) Hamada, M.; Ohtsuka, T.; Kawaida, R.; Koizumi, M.; Morita, K.; Furukawa, H.; Imanishi, T.; Miyagishi, M.; Taira, K. *Antisense Nucleic Acid Drug Dev.* **2002**, *12*, 301.
(49) Hrdlicka, P. J.; Babu, B. R.; Sorensen, M. D.; Harrit, N.; Wengel, J. *J. Am. Chem. Soc.* **2005**, *127*, 13293.
(50) Maag, H.; Schmidt, B.; Rose, S. J. *Tetrahedron Lett.* **1994**, *35*, 6449.
(51) Cuenoud, B.; Casset, F.; Hüsken, D.; Natt, F.; Wolf, R. M.; Altmann, K. H.; Martin, P.; Moser, H. E. *Angew. Chem., Int. Ed.* **1998**, *37*, 1288.
(52) Prakash, T. P.; Ask, P.; Lesnik, E.; Mohan, V.; Tereshko, V.; Egli, M.; Manoharan, M. *Org. Lett.* **2004**, *6*, 1971.
(53) Singh, S. K.; Kumar, R.; Wengel, J. *J. Org. Chem.* **1998**, *63*, 6078.
(54) Hrdlicka, P. J.; Kumar, T. S.; Wengel, J. *Chem. Comm.* **2005**, *34*, 4279.

Scheme 1. Structure (**A$_1$**)[a]

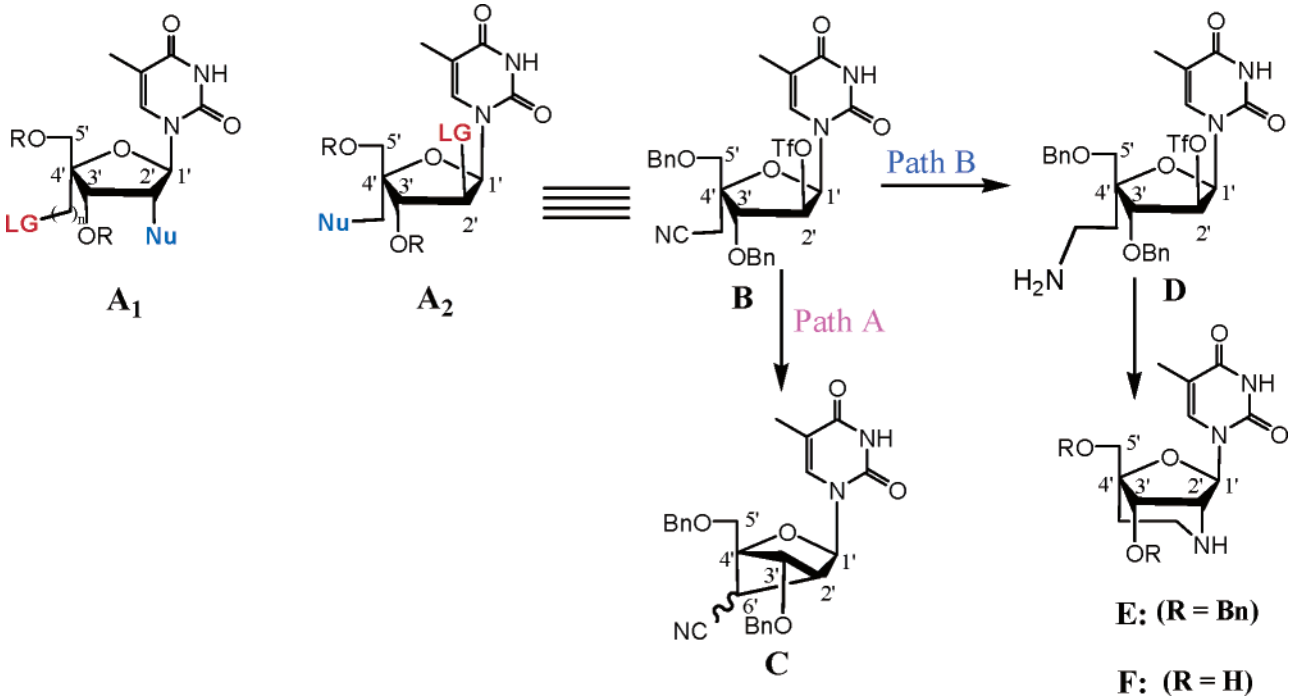

[a] General strategy for 2′,4′-cyclization thus far reported in the literature involves the engineering of a nucleophile (**Nu**) at C2′ and a leaving group (**LG**) at the extended arm of C4′. Structure (**A$_2$**), on the other hand, shows a reverse strategy in which the leaving group **LG** is placed in the sugar moiety, whereas the nucleophile **Nu** is engineered at the sidearm. Structure (**B**): Our strategy involving intermediate **A$_2$** involves a ring-closure reaction (path A) to give cyanomethylene-bridged carbocyclic nucleoside (**C**), through a α-carbanion, or alternatively involving path B, where CN is first reduced to putative (**D**) followed by instantaneous cyclization to give 2′,4′-conformationally constrained 2′-*N*,4′-*C*-ethylene-bridged aza-ENA-T (structure **E**). Both path A and B however involve a nucleophile at C4′ (**Nu**) and a departing group at C2′ (**LG**).

Table 1. Aza-ENA-T-Modified AONs and the Thermal Denaturation Studies of Their Duplexes with Complementary RNA or DNA Targets[a]

AON	AON sequences synthesized	T_m (°C with RNA)	ΔT_m	T_m (°C with DNA)	ΔT_m*	MALDI–MS of AON 1–5: found/calcd $[M + H]^+$
1	3′-d(CTTCTTTTTTACTTC)-5′	44		45		4448.6/4448.7
2	3′-d(CT**T**CTTTTTTACTTC)	48	+4	44.5	−0.5	4489.7/4491.1[b]
3	3′-d(CTTCT**T**TTTTACTTC)	46.5	+2.5	42.5	−2.5	4489.7/4490.7
4	3′-d(CTTCTTT**T**TTACTTC)	47.5	+3.5	42	−3	4489.7/4490.7
5	3′-d(CTTCTTTTT**T**ACTTC)	48	+4	42	−3	4489.7/4490.8

[a] T_m values measured as the maximum of the first derivative of the melting curve (A_{260} versus temperature) recorded in medium salt buffer (60 mM Tris-HCl at pH 7.5, 60 mM KCl, 0.8 mM $MgCl_2$, and 2 mM DTT) with a temperature range of 20−70 °C using 1 μM concentrations of the two complementary strands. $\Delta T_m = T_m$ relative to RNA compliment. $\Delta T_m^* = T_m$ relative to DNA compliment. **T** = aza-ENA-T monomer. [b] $[M + 2H]^+$.

considered an alternative strategy (general structure "**A$_2$**" in Scheme 1) for nucleophilic ring closure to give desired constrained nucleosides. An intermediate such as **B** in Scheme 1 can potentially lead us to two types of products, depending upon whether we generate a carbanion at the α carbon to the cyano group (path A in Scheme 1) or successfully reduce the cyano to the primary amino group without generating a α carbanion next to the −CN (path B in Scheme 1). We argued that, in the former case, we might be able to engineer the construction of a cyanomethylene-bridged carbocyclic [2.1.1] system (**C**) and that, in the latter case, it could lead us to the 2′-deoxy-2′-*N*,4′-*C*-ethylene-bridged nucleoside (aza-ENA-T) having a 2-aza-6-oxabicyclo[3.2.1]octane skeleton.

Thus, upon treatment of the intermediate (**B**) (Scheme 1) with NaHMDS in anhydrous tetrahydrofuran (THF), we found the formation of a stable fused product (**C**) (Scheme 1) with a 35% yield as a mixture of two diastereomers (*R*/*S*, 8:2) because of chiral C6′ (Scheme 1). The stereochemistry at C6′ in compound **C** has been proven by 2D correlation spectroscopy (COSY) and ^{1}H-homodecoupling experiments (parts a−c of Figure S13 and parts a and b of S14 in the Supporting Information). In the major diastereomer, the H3′ appears as a double doublet (dd, $J = 7.7$ and 1.5 Hz) because of the vicinal $^3J_{H3',H2'}$ coupling (7.7 Hz) with H2′ and, most importantly, a $^4J_{HH}$ W coupling with H6′ (1.5 Hz), which is only possible when C6′ is in the *R* configuration (Figure S49 in the Supporting Information). As a result of the *R* configuration at C6′, the dihedral angle between H6′ and H2′, ϕ(H6′−C6′−C2′−H2′), becomes very close to 90° (see the energy-minimized models in Figure S49 in the Supporting Information), which is why no vicinal three-bond coupling between H6′ and H2′ ($^3J_{H2',H6'}$) has been observed for the major diastereomer. This means that the C6′ in the minor diastereomer is in the *S* stereochemistry (for a model, see Figure S49 in the Supporting Information). The observed significant upfield ^{13}C chemical shift at the C1′ (63.6 ppm) in the fused product (**C**) is probably due to a change from the more electronegative 2′-OTf to the 2′-deoxy-2′-*C* (carbocyclic) conjugate, resulting in an increase of the anomeric effect in the highly constrained North-fused nucleoside as well as a +I effect owing to the carbon substituent at C2′. Finally, the 1D difference

Scheme 2. Reagents and Conditions[a]

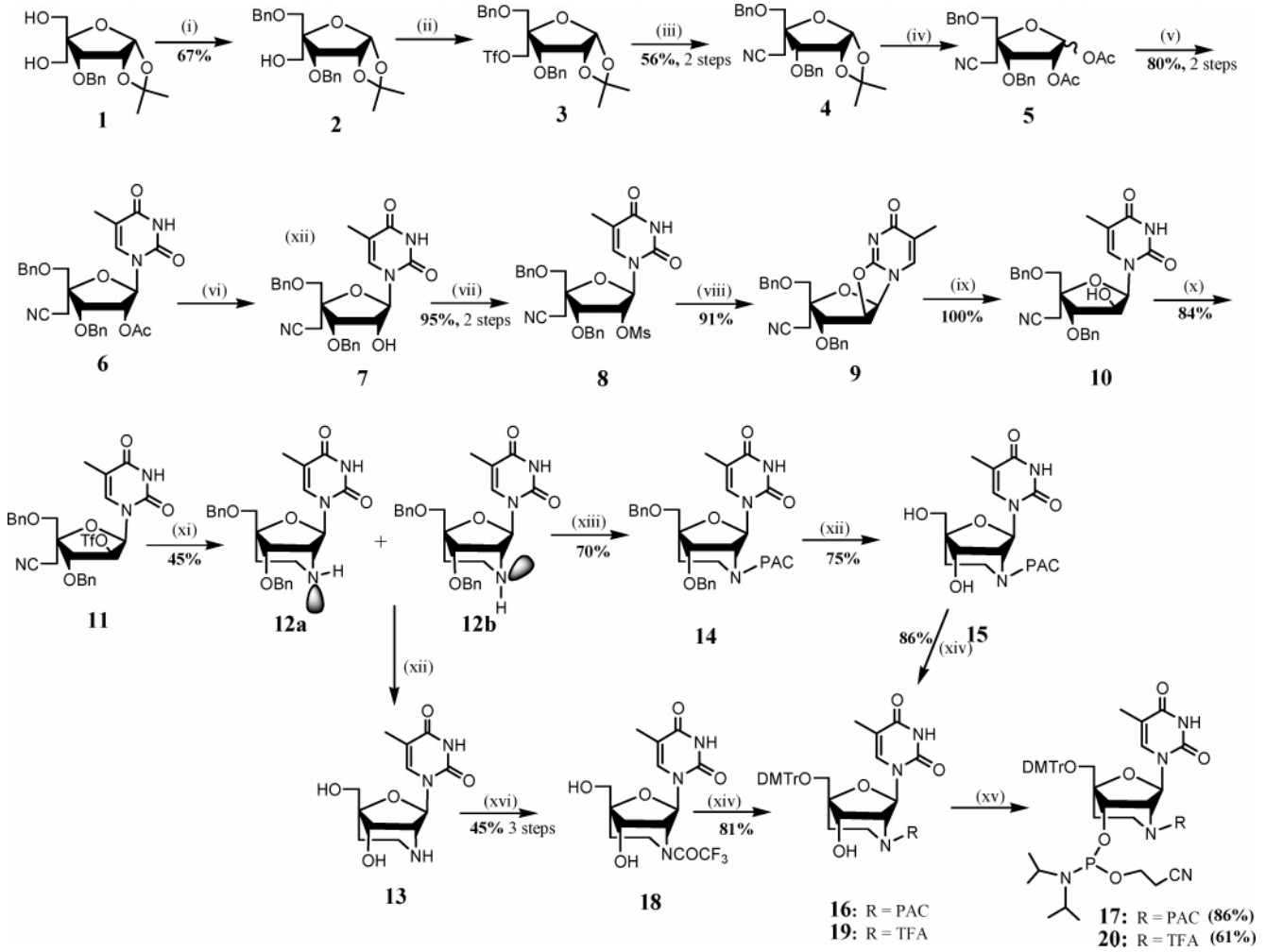

[a] (i) NaH, BnBr, CH_3CN, −5 °C to room temperature, overnight; (ii) Tf_2O, pyridine, CH_2Cl_2, 0 °C, 3 h; (iii) LiCN, DMF, room temperature, 3 days; (iv) acetic acid, Ac_2O, triflic acid, room temperature, 3 h; (v) persilylated thymine, TMSOTf, CH_3CN, 80 °C, overnight; (vi) NaOMe, methanol, 3 h; (vii) MsCl, pyridine, 0 °C, 6 h; (viii) DBU, CH_3CN, room temperature, 1 h; (ix) 0.1 M H_2SO_4, acetone, reflux, overnight; (x) Tf_2O, pyridine, CH_2Cl_2, DMAP, 0 °C, 2.5 h; (xi) $NaBH_4$, trifluoroacetic acid, THF, room temperature, overnight; (xii) $Pd(OH)_2$, ammonium formate, methanol, reflux, overnight, followed by 1 M BCl_3 in CH_2Cl_2, −78 °C, 3 h; (xii) phenoxyacetyl chloride, pyridine, room temperature, 3 h; (xiv) DMTr-Cl, pyridine, room temperature, 7 h (overnight for **19**); (xv) $NC(CH_2)_2OP(Cl)N(^iPr)_2$, DIPEA, THF, room temperature, 3 h (overnight for **20**). Abbreviations: Bn, benzyl; Ac, acetyl; Tf, trifluoromethylsulfonyl; PAC, phenoxyacetyl; THF, tetrahydrofuran; DBU, 1,8-diazabicyclo[5.4.0]undec-7-en; DMTr, 4,4′-dimethoxytrityl; DIPEA, diisopropylethylamine; TFA, trifluoroacetyl.

nuclear Overhauser effect (NOE) experiment is consistent with the North-type sugar conformation (see ii in Figure S2 and Figure S10 in the Supporting Information).

The structural integrity of this conformationally constrained product was also proven by a ^1H-^{13}C NMR correlation (HMBC) experiment (see i in Figure S2 in the Supporting Information), which showed C2′/H6′ ($^2J_{CH}$), through bond correlation. The mass-spectral data by matrix-assisted laser desorption ionization−time of flight (MALDI−TOF) have also provided evidence for the structural integrity of the highly strained carbocyclic nucleoside (see the Experimental Section for full characterization). However, our efforts to remove the benzyl group from compound **C** using $Pd(OH)_2/HCOONH_4$ and BCl_3 (Scheme 1) has not met with success thus far. The other problem that remains is to find a mild reducing agent, which can convert the −CN group in compound **C** (Scheme 1) to a relatively poorer electron-withdrawing group (for example, to an amino function), to assess its potential in the strategies concerning gene-directed drug development [reduction by $(CF_3CO_2)_3BH$ was unsuccessful].

These initial unsuccessful efforts to proceed through path A in Scheme 1 have made us explore the feasibility of structure **B** (path B in Scheme 1), which has a masked amino function in the form of a −CN group in the side arm as well as a $-CH_2-$ for one carbon homologation (**D** in Scheme 1), both of which are necessary for intramolecular cyclization to yield a novel aza-ENA-T nucleoside (compound **E**, Scheme 1). The complete synthetic strategy, which leads us to the successful synthesis of aza-ENA-T, is shown in Scheme 2. It is also noteworthy that the aliphatic nitrile ($pK_a \sim 29-31$)[55] derivatives (**4**−**11**, Scheme 2) were fully compatible with the synthetic strategy containing strongly acidic and basic conditions as described in Scheme 2.

1. Synthesis of Aza-ENA-T. The synthesis of the aza-ENA-T derivative was started with a known sugar precursor[21] **1**, which was converted to 3,5-di-*O*-benzyl-4-*C*-hydroxymethyl-1,2-*O*-isopropylidene-α-D-ribofuranose **2**.[21] Compound **2** was then converted to the 4-triflyloxymethylene derivative **3** using triflic

(55) Fleming, F. F.; Shook, B. C. *Tetrahedron* **2002**, *58*, 1.

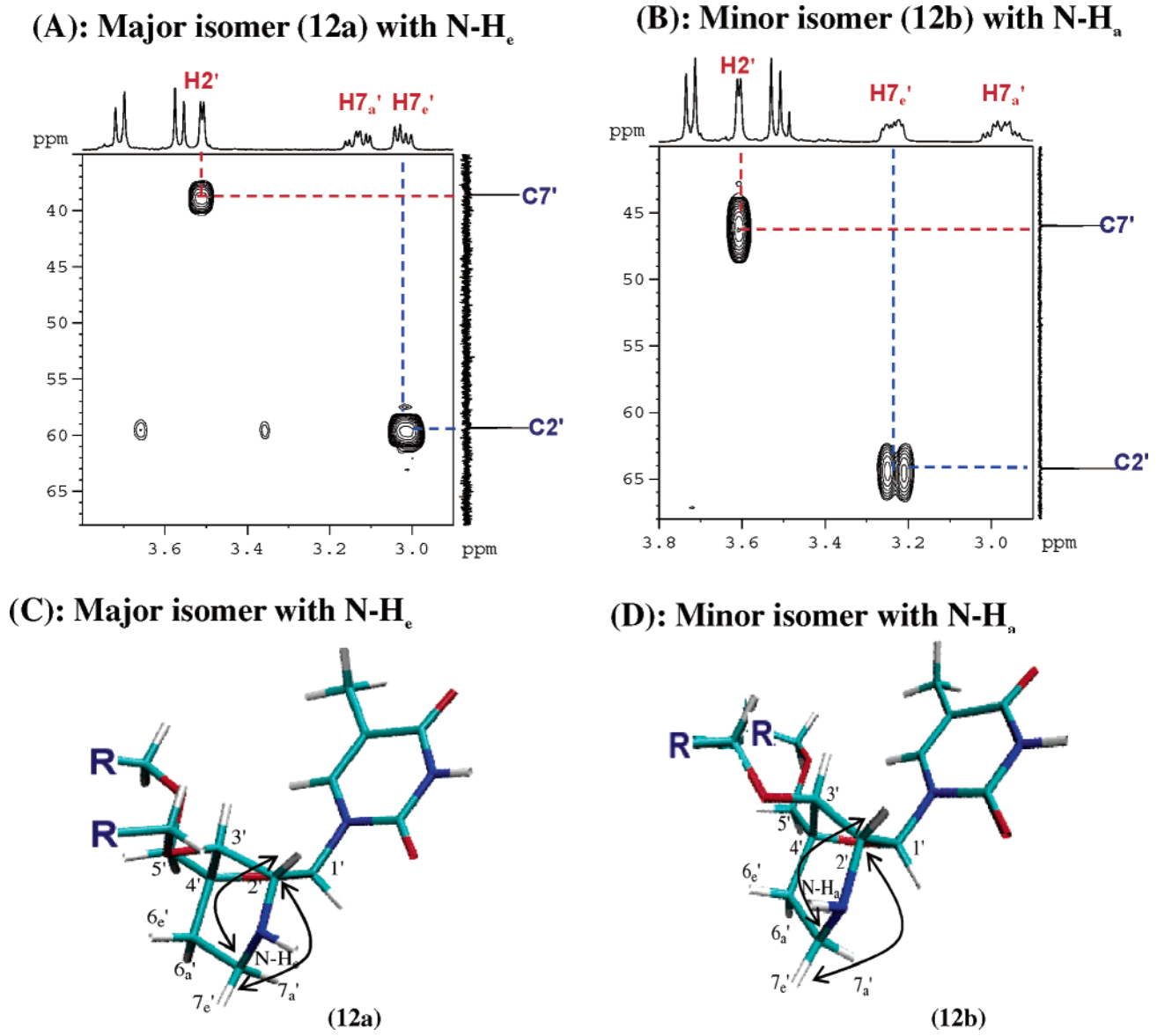

Figure 1. (A and B) ^{1}H-^{13}C HMBC spectra, showing the long-range through-bond connectivities between C7′/H2′ and C2′/H7$_e$′ for the two diastereomers **12a** and **12b**. (C and D) Energy-minimized stereochemical representations, showing the ^{1}H-^{13}C HMBC connectivities of the two diastereomers **12a** and **12b**; R = OCH_2Ph (not shown).

anhydride in a dichloromethane/pyridine mixture (3:1, v/v) at 0 °C. The crude product obtained after aqueous workup was subsequently treated with 3 equiv of LiCN in *N*,*N*-dimethylformamide (DMF) and stirred at room temperature for 3 days, which afforded the cyano-sugar **4** in an overall yield of 56% from **2**, along with some unidentified minor compounds. Compound **4** was converted to diacetate **5** (1,2-di-*O*-acetyl-3,5-di-*O*-benzyl-4-*C*-cyanomethyl-D-ribofuranose) using a mixture of acetic acid, acetic anhydride, and triflic acid by stirring for 3 h at room temperature. The crude product **5** (**4** → **5** was almost quantitative) was subjected to the modified Vorbruggen reaction[31,56] using *in situ* silylation of thymine and subsequent trimethylsilyl triflate mediated coupling to give the β-configured thymine nucleoside **6** in 80% yield. The β configuration of **6** was confirmed by a 1D differential NOE experiment, which showed 8% NOE enhancement of H6 upon irradiation of H2′ ($d_{H6-H2'} \approx 2.7$ Å for β anomer, and $d_{H6-H2'} \approx 4$ Å for α anomer). Deacetylation of **6** at C2′ was carried out using sodium methoxide in methanol at room temperature, and the product (**7**) was isolated as a crude material [single spot on thin-layer chromatography (TLC); for ^{13}C NMR, see Figure S17 in the Supporting Information], which was directly mesylated using mesyl chloride in pyridine at room temperature to afford **8** with an overall yield of 95% in two steps from **6**. The compound **8** was converted to the 2,2′-anhydro product **9** using 1.05 equiv of 1,8-diazabicyclo[5.4.0]undec-7-ene (DBU) in acetonitrile in 91% yield. It should be noted that the use of excess base or stronger base such as NaHMDS resulted in instantaneous depyrimidation. Opening of the 2,2′-anhydro ring in **9** went smoothly by refluxing with a mixture of 0.1 M aqueous sulfuric acid/acetone (1:1, v/v) to give the *arabino* product (**10**) quantitatively.

Treatment of **10** with triflic anhydride, pyridine, 4-dimethylaminopyridine (DMAP), and anhydrous CH_2Cl_2 at 0 °C gave the desired triflate nucleoside **11** in 84% yield. Reduction of

(56) Vorbrüggen, H.; Höfle, G. *Chem. Ber.* **1981**, *114*, 1256.

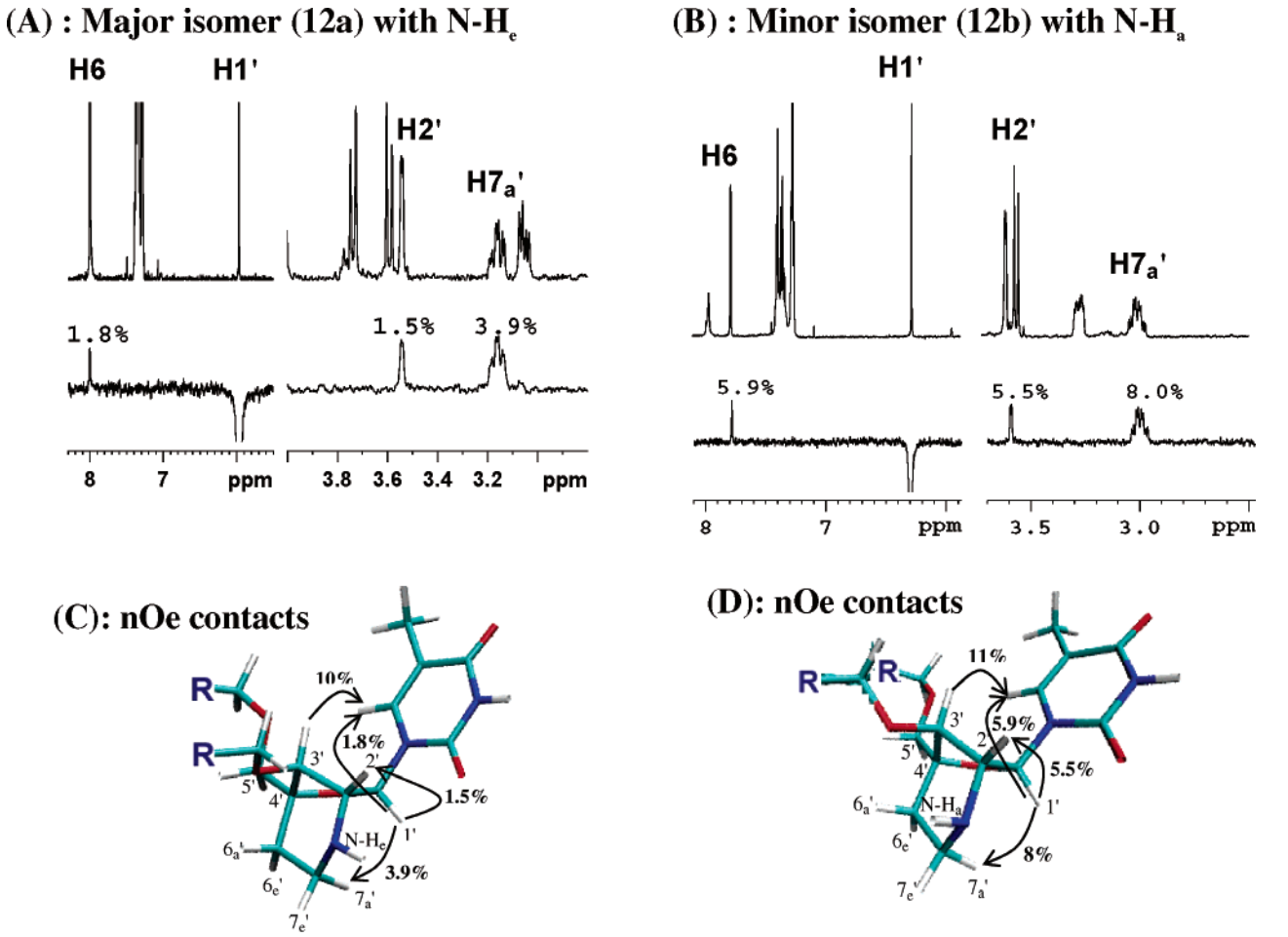

Figure 2. One-dimensional selective NOESY spectra of **12a** and **12b**. (A) Irradiation at H1′ in **12a** shows enhancements at H7$_a$′ (3.9%), H2′ (1.5%), and H6 (1.8%). (B) Irradiation at H1′ in **12b** shows enhancements at H7$_a$′ (8.0%), H2′ (5.5%), and H6 (5.9%). (C and D) NOE contacts in the two diastereomers **12a** and **12b**, respectively (R = $OCH_2\underline{Ph}$ and are not shown for clarity of the picture).

the cyano group using trifluoroacetoxy borohydride,[57] prepared *in situ* from $NaBH_4$ and trifluoroacetic acid, gave the primary amine, which spontaneously resulted in intramolecular cyclization to give a mixture of two diastereomeric aza-ENA-T **12a** and **12b** isomers, isolated in 40 and 5% yield, respectively. These diastereomers showed identical masses by MALDI−TOF mass spectroscopy (see the Experimental Section). The fact that the intramolecular ring-closure reaction has indeed taken place to give the 2′-deoxy-2′-*N*,4′-*C*-ethylene-bridged nucleoside (aza-ENA-T) having a 2-aza-6-oxabicyclo[3.2.1]octane skeleton fused with a North-conformationally constrained pentofuranosyl moiety in **12a** and **12b** was unequivocally proven by long-range ^{1}H-^{13}C NMR correlation (HMBC, Figure 1) and NOE experiments (Figure 2). The benzyl groups of the diasteromeric **12a**/**12b** were deprotected for characterization using $Pd(OH)_2$/ammonium formate in methanol and subsequently BCl_3 in dichloromethane at −78 °C to aza-ENA-T (**13**) in 60% yield (Scheme 2).

2. NMR Characterization of 12a, 12b, and 13. The characterization and conformational analysis of **12a**, **12b**, and **13** have been performed using NMR data (at 500 and 600 MHz in $CDCl_3$/DMSO-d_6) obtained by double homodecoupling experiments, 1D nuclear Overhauser effect spectrometry (NOESY),[58,59] 1D selective total correlation spectroscopy (TOCSY),[59] and ^{13}C NMR experiments, including distortionless enhancement by polarization transfer (DEPT),[60] as well as long-range ^{1}H-^{13}C HMBC correlation ($^2J_{H,C}$ and $^3J_{H,C}$)[61] and a one-bond heteronuclear multiple-quantum coherence (HMQC) experiment.[62]

2.1. Assignment of ^{1}H and ^{13}C Chemical Shifts and Evidence for Ring Closure in 12a, 12b, and 13. The COSY and HMQC experiments allowed us to assign the ^{1}H and ^{13}C chemical shifts for **12a**, **12b**, and **13** (see Figures S23, S25, S28, and S30 in the Supporting Information). The HMBC spectrum for **12a**, **12b**, and **13** showed that only H7$_e$′ (equatorial H7′) has a correlation with C2′ but none between H7$_a$′ (axial H7′) and C2′. This suggested that the dihedral angle between H7$_e$′ and C2′, ϕ[H7$_e$′−C7′−N−C2′], is close to 180°, whereas the dihedral angle between H7$_a$′ and C2′, ϕ[H7$_a$′−C7′−N−C2′], is about 90°. The presence of a long-range HMBC correlation of H7$_e$′ with C2′ also unequivocally showed that the six-membered piperidino[3.2.1] ring fused with the pentofuranose ring has indeed been formed in the ring-closure reaction (**11** →

(57) Gruenefeld, P.; Richert, C., *J. Org. Chem.* **2004**, *69*, 7543.
(58) Kessler, H.; Oschkinat, H.; Griesinger, C.; Bermel, W. *J. Magn. Reson.* **1986**, *70*, 106.
(59) Stonehouse, J.; Adell, P.; Keeler, J.; Shaka, A. J. *J. Am. Chem. Soc.* **1994**, *116*, 6037.
(60) Doddrell, D. M.; Pegg, D. T.; Bendall, M. R. *J. Magn. Reson.* **1982**, *48*, 323.
(61) Bax, A.; Summers, M. *J. Am. Chem. Soc.* **1986**, *108*, 2093.
(62) Bax, A.; Geriffey, R.; Hawkins, B. *J. Magn. Reson.* **1983**, *55*, 301.

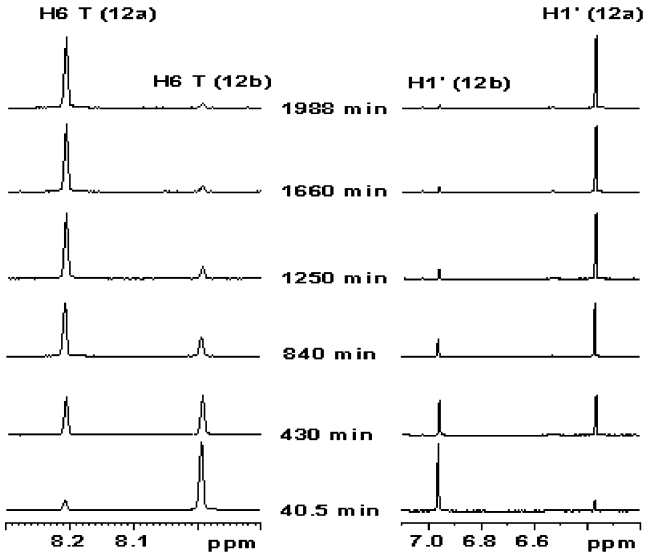

Figure 3. Nonreversible conversion of **12b** (with NH_a) to **12a** (with NH_e) in pyridine-d_5 at 298 K.

12a/**12b**, Scheme 2). The deprotected **13** showed very similar NMR spectra as that of the major isomer **12a** (see Figure S37 in the Supporting Information). The 1D selective TOCSY experiment confirmed the spin system for $H7_a'$, $H7_e'$, and $H6_a'$, for **12a** and **13**, whereas an additional correlation for $H7_a'$, $H7_e'$, $H6_a'$, and $H6_e'$, with the NH proton at δ 4.55 ppm was also found for **12b**. The presence of the NH proton was also confirmed by D_2O exchange and NMR simulation experiments. The $H7_a'$ has three vicinal couplings ($^3J_{H7a',H6a'} = 11.9$ Hz, $^3J_{H7a',H6e'} = 5.2$ Hz, and $^3J_{H7a',NH} = 11.9$ Hz) besides the geminal coupling ($^2J_{H7a',H7e'} = 14.2$ Hz). This suggests that the NH proton in **12b** is in an axial orientation (NH_a) and that the NH proton in **12a** is in the equatorial configuration. The vicinal coupling of the NH proton in **12a** with neither $H7_a'$ nor $H7_e'$ has however been observable by NMR, probably because of the fast exchange with the bulk solvent. Details of the assignments of proton resonances and stereochemistry for **12a**, **12b**, and **13** can be found in Discussion S3 in the Supporting Information.

3. Conversion of Minor 2′-NH_a-Diastereomer (12b) to the Major 2′-NH_e-Diastereomer (12a): Kinetics and Conformational Studies of Nitrogen Inversion. Diastereomers **12a** and **12b** have been isolated in pure form and fully characterized by NMR and mass spectroscopy, suggesting that these isomers were fairly stable in CH_2Cl_2 containing ca. 5−10% methanol or in $CHCl_3$ solution. The piperidino moiety in the major isomer (**12a**) takes up the chair conformation with N−H equatorial (NH_e) (see Discussion S3 in the Supporting Information) to reduce the 1,3-diaxial interaction, whereas the minor isomer (**12b**), with the piperidino ring also in the chair conformation but with axial N−H (NH_a) (see Discussion S3 in the Supporting Information), is relatively unstable because of the unfavorable 1,3-diaxial interaction (see below).

Thus, in pyridine-d_5 (Figure 3), the minor isomer (**12b**) was found to have converted almost completely (>99%) to the major isomer (**12a**) in 33 h at 298 K and no reverse isomerism was observed starting from the major isomer (**12a**) under our experimental conditions. We have subsequently determined the rate of inversion at 293 K ($k = 1.0 \times 10^{-5}$ s^{-1}), 298 K ($k = 4.4 \times 10^{-5}$ s^{-1}), 303 K ($k = 8.0 \times 10^{-5}$ s^{-1}), 308 K ($k = 1.0 \times 10^{-4}$ s^{-1}), and 318 K ($k = 4.0 \times 10^{-4}$ s^{-1}), respectively,

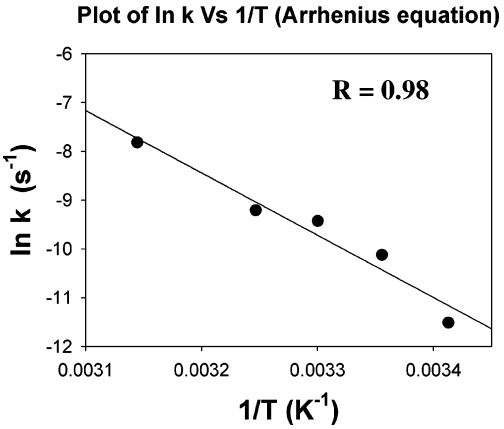

Figure 4. Determination of activation energy (E_a) for the nitrogen inversion of **12b** to **12a** using an Arrhenius plot of ln k versus $1/T$.

using the equation of the unimolecular first-order rate kinetics.[63] The populations of **12a** and **12b** at different time intervals were obtained from the peak integrals of H6 for the two isomers.

The Arrhenius plot of ln k versus $1/T$ shows a linear correlation with $R = 0.98$. The slope gave $E_a = 25.4$ kcal mol^{-1}, whereas the intercept showed the frequency of the collision factor $A = 1.190 \times 10^{14}$ s^{-1} (Figure 4). The free energy of activation was also calculated,[64] which was found to be $\Delta G^{\ddagger} = 23.4$ kcal mol^{-1} at 298 K in pyridine-d_5. In $CDCl_3$, the two diastereomers **12a** and **12b** have very slowly (in 30 days) reached an equilibrium (40:60 of **12a**/**12b**) with the equilibrium constant[63] $K_c = 0.67$. The $\Delta G^{\ddagger}$ was found to be 25.4 kcal mol^{-1} at 298 K (Figure S43 in the Supporting Information). The complete conversion in pyridine-d_5 with a 2 kcal mol^{-1} lower $\Delta G^{\ddagger}$ suggests that the conversion of **12b** to **12a** is base-catalyzed.

The factors that influence inversion at pyramidal nitrogen in bicylic amines have been discussed for several decades.[65] Usual values of nitrogen inversion barriers for alicyclic amines lie in the 5−9 kcal mol^{-1} range.[65,66] However, abnormal barriers (>13 kcal mol^{-1}) were found for azanorbornanes, which has been implied to nitrogen inversion C−N rotation (NIR), the "bicyclic effect".[65,67,68] Despite several attempts, the mechanistic reason for this bicyclic effect could not be satisfactory explained in terms of steric interactions or ring strain.[69] Only in crowded systems such as N-*t*-Bu azanorbornanes could steric interactions be sufficiently strong enough to play an important factor. The nitrogen inversion rotation barrier determined among a set of various categories of bicyclic amines using dynamic NMR and MP2/6-31G* is found to vary from 6.4 to 13 kcal mol^{-1}.[68] Several interesting conclusions have thus far emerged from various works[66,68] on nitrogen inversion and bicyclic effect in cyclic amines: (1) The NIR barriers increase with a decrease of the ring size in azabicycles. (2) The presence of a five-

(63) Atkins, P.; de Paula, J., *Atkin's Physical Chemistry*, 7th ed.; Oxford University Press: New York, 2002.
(64) Inezedy, J.; Lengyel, T.; Ure, A. M. *IUPAC Compendium of Analytical Nomenclature*, 3rd ed.; Blackwell Science, Oxford, U.K., 1997; p 15.
(65) Lehn, J. M. *Chem. Forsch.* **1970**, *15*, 311.
(66) Belostotskii, A. M.; Gottlieb, H. E.; Hassner, A. *J. Am. Chem. Soc.* **1996**, *118*, 7783.
(67) Nelsen, S. F.; Ippoliti, J. T.; Frigo, T. B.; Petillo, P. A. *J. Am. Chem. Soc.* **1989**, *111*, 1776.
(68) Belostotskii, A. M.; Gottlieb, H. E.; Shokhen, M. *J. Org. Chem.* **2002**, *67*, 9257.
(69) Davies, J. W.; Malpass, J. R.; Moss, R. E. *Tetrahedron Lett.* **1985**, *26*, 4533.

membered ring as a component of a rigid nitrogen-bridged bicyclic skeleton increases the NIR barrier by ca. 3 kcal mol^{-1} per ring, thereby showing a relationship between azabicycle geometry and the NIR barrier. (3) The flattening of the nitrogen pyramid, for example, through the introduction of a double bond in the six-membered ring as a component of a rigid nitrogen-bridged bicyclic skeleton, decreases the NIR barrier of the ring inversion. (4) It has been evidenced by dynamic NMR at ~180 K that the ring inversion in the rigid nitrogen-bridged bicyclic skeleton involves interconversion of conformers with equatorial and axial *N*-alkyl substituents. (5) Although an earlier suggestion that high strain, which develops during NIR for the endocyclic CNC angle change from N-pyramid, is responsible for the bicyclic effect, no satisfactory correlation has been however found between NIR barriers and the CNC angle for different bicyclic amines. No experimental evidence has been found thus far to support the suggestion that the observed high NIR barriers in the constrained amines is caused by the delocalization of the N lone pair.

In conclusion, the high $\Delta G^{\ddagger}$ found 23.4 kcal mol^{-1} at 298 K for the conversion of axial N−H containing isomer **12b** to the energetically stable equatorial N−H containing isomer **12a** is unique in the long history[65,67,68] of abnormally high activation barriers for nitrogen inversion. This also constitutes the first example in which both the piperidine isomers with the axial and equatorial lone-pair orientation have been isolated in the pure form and fully characterized by NMR and mass spectroscopy.

4. Molecular Structure of the Aza-ENA-T Derivatives 12a, 12b, and 13 Based on NMR, *ab initio*, and Molecular Dynamics (MD) Calculations. The experimental coupling constants from 600 MHz spectra of the 3′,5′-*bis*-OBn-protected (**12a** and **12b**) and fully deprotected (**13**) aza-ENA-T compounds have been further analyzed to build up their molecular structures using the following protocol: (i) Derive initial dihedral angles from the observed[3] J_{HH} using the Haasnoot−de Leeuw−Altona generalized Karplus equation[70,71] (Table S6 in the Supporting Information). (ii) Perform NMR-constrained MD simulation (0.5 ns, 10 steps) simulated annealing (SA) followed by 0.5 ns of NMR-constrained simulations at 298 K using the NMR-derived torsional constraints from step (i) to yield NMR-defined molecular structures of 3′,5′-*bis*-OBn-protected (**12a** and **12b**) and deprotected aza-ENA-T (**13**) (for details of theoretical simulations, see the Supporting Information). Our conclusions based on detailed MD, SA, and *ab initio* simulations are as follows (for full details, see Tables S6 and S7 and Figures S44, S45, and S46 in the Supporting Information).

4.1. Sugar Pucker Conformation. Non-observable $^3J_{H1',H2'}$ and low $^3J_{H2',H3'}$ (Tables S3 and S6 in the Supporting Information) experimental coupling indicate that, similar to that in the ENA,[22] LNA,[22,23] and 2′-amino LNA,[25] the piperidino modification of the sugar moiety in aza-ENA-T restricts sugar pucker to the North-type conformation (for details, see Tables S6 and S7 and Figure S44 in the Supporting Information). *Ab initio* and MD simulations (Tables S6 and S7 in the Supporting Information) have shown that the sugar moiety is indeed conformationally restricted to the North conformation (pseudorotational phase angle $P = 14 \pm 7°$ for **12a** and **12b** and $19 \pm 8°$ for **13**, sugar puckering amplitude $\phi_m = 48 \pm 4°$ for **12a**, **12b**, and **13**; Table S7 in the Supporting Information), and the sugar pucker in aza-ENA-T is close to that of the ENA and LNA ($P = 12-19°$),[22] however, with the sugar puckering amplitude, ϕ_m, lower by ~10° ($\phi_m \approx 46°$) compared to that of the LNA ($\phi_m \approx 56°$).[22,23] ENA-T and aza-ENA-T have also showed very similar conformational dynamics with 5−8° of variation of the sugar torsions along the MD trajectories (Table S7 in the Supporting Information), and the sugar atom position root-mean-square deviation (RMSD) is less than 0.1 Å (Figure S46 in the Supporting Information).

4.2. Conformation of the Piperidino Ring. *Ab initio* and MD simulations, a 1D NOESY experiment (Figure 2), as well as dihedral angles obtained using the generalized Karplus equation[70,71] (shown in Figure S45 in the Supporting Information) point to the chair conformation for the piperidino heterocycle. Both the sugar and piperidino rings of aza-ENA-T show exceptional rigidity, with rmsd values of the sugar and piperidino exocylic heavy (C, N, and O) atoms being less than 0.09 Å (Figure S46 in the Supporting Information) along the MD trajectories. Higher dynamics have been observed for the base (RMSD of about 0.7 Å) of aza-ENA-T (**12a**, **12b**, and **13**), while flanking OBn groups in the 3′,5′-*bis*-OBn-protected aza-ENA-T compounds **12a** and **12b** (RMSD of 1.3−1.7 Å; Figure S46 in the Supporting Information) are expectedly found to be the most dynamic parts of these protected compounds.

5. Preparation of Aza-ENA-T Phosphoramidite for AON Synthesis. We have then prepared both the *N*-phenoxyacetyl (PAC)- and *N*-trifluoroacetyl-protected aza-ENA-T phosphoramidite blocks **17** and **20** from **12a**/**12b** to synthesize aza-ENA-T-incorporated AONs (Scheme 2).

The aza-ENA-T analogue **12a**/**12b** was N-protected using PAC-Cl in pyridine, affording **14** (70%) as a mixture of rotamers because of the restricted rotation of the amide bond of PAC. Debenzylation of **14** was achieved by doing a successive reaction with $Pd(OH)_2$/ammonium formate in methanol and then with BCl_3 in anhydrous CH_2Cl_2 for 3 h to give **15** in 75% yield. Dimethoxytrytilation of 5′-OH in **15** using DMTr-Cl and pyridine followed by phosphytilation of 3′-OH using standard conditions[31] afforded **16** and **17** in 90 and 86%, respectively [^{31}P NMR of **17** ($CDCl_3$) δ: 150.7, 150.3, 149.2, and 148.1; see Figure S29 in the Supporting Information].

The phosphoramidite **17** was successfully incorporated into the mixed 15-mer sequence (Table 1), but to our surprise, the PAC-protecting group was very stable and could not be deprotected even in 33% aqueous ammonia and AMA [33% aqueous ammonia/methylamine, 1:1 (v/v)] at 65 °C for 2 days, which was clear from the mass measurement using MALDI−TOF mass spectroscopy (expected mass with PAC protection, *m*/*z* 4624.7; and observed, 4624.9). The PAC-protected nucleoside **15**, on the other hand, could be deprotected with aqueous ammonia at 55 °C overnight.

Because the PAC protection of the amino function of aza-ENA-T did not work satisfactorily in our hands, we incorporated a trifluoroacetyl-protecting group (Scheme 2), where the benzyls were first deprotected using the same condition as for **15** (Scheme 2). The deprotected nucleoside **13** was directly treated with an excess of ethyl trifluoroacetate in methanol at room temperature overnight to give the *N*-trifluoroacetyl-protected

(70) Haasnoot, C. A. G.; de Leeuw, F. A. A. M.; Altona, C. *Tetrahedron* **1980**, *36*, 2783.
(71) Altona, C.; Sundaralingam, M. *J. Am. Chem. Soc.* **1972**, *94*, 8205.

nucleoside **18** in 45% yield after 3 steps from **12** as a mixure of rotamers. Dimethoxytritylation and phosphitylation were carried out using the same conditions as for **16** and **17** in Scheme 2 to afford **19** in 81% yield and **20** in 61% yield as a mixture of four isomers [^{31}P NMR ($CDCl_3$) δ: 150.1, 149.9, 149.8, and 149.2; Figure S36 in the Supporting Information]. Phosphoramidite **20** was successfully incorporated at different positions of mixed 15-mer AON sequences (Table 1), using a standard phosphoramidite approach,[31] with a 10 min coupling time and a coupling efficiency of ~95%. Deprotection of all of the base-labile protecting groups went smoothly, with 33% aqueous ammonia at 55 °C as confirmed by MALDI−TOF mass spectroscopy (Table 1). All oligos were purified by polyacrylamide gel electrophoresis (PAGE) (20% polyacrylamide/7 M urea), extracted with 0.3 M NaOAc, and desalted with a C18 reverse-phase cartridge to give AONs in >99% purity.

6. Thermal Denaturation Studies of Aza-ENA-T-Modified AONs. The thermal stability of duplexes involving aza-ENA-Ts was determined by the complementary RNA and DNA as shown in Table 1. Single modifications were incorporated one at a time at different positions (Table 1) of the 15-nucleotide AON sequence, 3′-d(CTTCTTTTTTACTTC)-5′, to determine the sequence dependency in the target affinity. The results reveal (Table 1) that the single aza-ENA-T modification enhances the target affinity significantly with complementary RNA (ΔT_m = +2.5 to +4 °C), depending upon the site of the modification in the AON strand. This can be attributed to the site dependency of the variable conformational pre-organization imparted by the North-fused sugar moiety on the single-stranded AON. Even though the thermal stabilities of duplexes containing single ENA modifications were not reported,[22,42] we presume that aza-ENA-T will have slightly more favorable target affinity toward RNA than the isosteric ENA counterpart (double modification gave +3.5 °C per modification).[22] The 2′-amino function of aza-ENA-T is almost 50% protonated at the physiological pH considering its pK_a of 6.66 ± 0.03 compared to that of the 2′-amino-LNA counterpart (pK_a of 6.17 ± 0.03), determined using pH-dependent ^{1}H NMR measurements[72] (see the Experimental Methods and Figure S48 in the Supporting Information for details). This means that the aza-ENA-T- or 2′-amino-LNA-T-incorporated AONs can have an electrostatic interaction with the neighboring phosphate at the physiological pH, which favors efficient duplex formation as observed in azetidine-modified AONs.[31] On the other hand, with complementary DNA, there was a significant drop in duplex melting. This can be due to the 2′,4′-ethylene bridge, which causes a steric clash in the minor groove of the AON−DNA duplex.

7. RNase H Digestion Studies of Aza-ENA-T-Modified AON/RNA Heteroduplexes. *Escherichia coli* RNase H1 has been used in this work because of two reasons: first, it is commercially available in a pure form, and second, its cleavage properties are not very different from those of the mammalian enzyme.[73] Hence, the antisense properties of aza-ENA-T-modified oligonucleotides in duplex with the complementary RNA were compared with the native as well as with the identical oxetane-modified counterparts,[74] with *E. coli* RNase H1 as a model system. Four different aza-ENA-T-containing AON mixtures, each obtained by incorporating single aza-ENA-T modification at one of the four different positions (AONs 2−5 in Table 1), of identical DNA sequence, when formed duplex with the complementary RNA, were found to be excellent substrates for RNase H1 but with varying RNA cleavage sites depending upon the site of modification on the AON strand. We have previously reported the RNase H1 digestion properties of oxetane-modified AON/RNA hybrid duplexes in an identical sequence.[74] The RNA cleavage patterns of all aza-ENA-T-modified AONs (AON 2−5 in Table 1) were found to be uniquely *different* from those of the isosequential oxetane-modified AONs (AON 6−9; Figure 6). AON 2 showed only one prominent cleavage site at the A8 position of the complementary RNA (Figure 5), unlike the oxetane-modified AON 6, which showed cleavages at A7, A8, A10, and U11, with no clear preferences (Figure 6). A comparison of AON 4 versus AON 8 and AON 5 versus AON 9 clearly shows the absence of a single RNA cleavage site in aza-ENA-T-modified AONs/RNA duplexes compared to those of the oxetane-modified counterparts (A7 of AON 8 and A9 of AON 9). AON 3 and its isosequential oxetane analogue AON 7, on the other hand, showed an identical cleavage footprint pattern of a 5-nucleotide gap. This shows that the local structures of all aza-ENA-T-modified AONs/RNA duplexes are not the same. The RNase H enzyme indeed can finely discriminate these local variations of the stereochemical properties of the microstructure brought about by various types and incorporation sites of the North-type modification (aza-ENA-T versus oxetane modifications) in the AON. These local structure variations were however not observable by circular dichroism (CD) spectra (see Figure S3 and Discussion S4 in the Supporting Information).

This shows that the certain specific flexibility of the AON/RNA duplex and accessibility of the RNA strand in the heteroduplex is required for RNase H binding and cleavage. The RNase H1 recruitment capability for LNA-modified AONs were reported earlier,[73] which showed a minimum gap of 7−8 DNA monomers to induce full cleavage activity. This difference in RNase H activity between the LNA-, oxetane-, and aza-ENA-T-modified AONs/RNA duplexes can be due to the difference in the conformational flexibility as well as the resulting hydration pattern in the minor groove imparted by the fused four-, five-, and six-membered rings locked to the pentofuranose ring.

Finally, to evaluate the cleavage rate, quantification of gels was performed densitometrically and the uncleaved RNA fraction was plotted as a function of the incubation time (Figure 5B). The enzyme digestion experiment was performed at a lower enzyme concentration (0.08 unit) to observe the cleavage rate (see Figure S4 in the Supporting Information).

Reaction rates were determined by fitting to single-exponential decay functions. Recently, Kurreck et al.[73] have shown that the RNase H cleavage efficiency of AON can be correlated with its affinity toward target RNA. The relative cleavage rates with aza-ENA-T-modified AON/RNA duplex were however quite comparable to that of the native counterpart (Table S1 in the Supporting Information and parts B and D in Figure 5).

8. Stability of Aza-ENA-T/DNA Chimeras in Human Serum. The stability of AON in cells toward various exo- and endonucleases is warranted to fulfill the requirements for an ideal *antisense* agent.[6] The stabilities of aza-ENA-T-modified

(72) Acharya, S.; Barman, J.; Cheruku, P.; Chatterjee, S.; Acharya, P.; Isaksson, J.; Chattopadhyaya, J. *J. Am. Chem. Soc.* **2004**, *126*, 8674.
(73) Kurreck, J.; Wyszko, E.; Gillen, C.; Erdmann, V. A. *Nucleic Acids Res.* **2002**, *30*, 1911.
(74) Pradeepkumar, P. I.; Zamaratski, E.; Foldesi, A.; Chattopadhyaya, J. *Tetrahedron Lett.* **2000**, *41*, 8601.

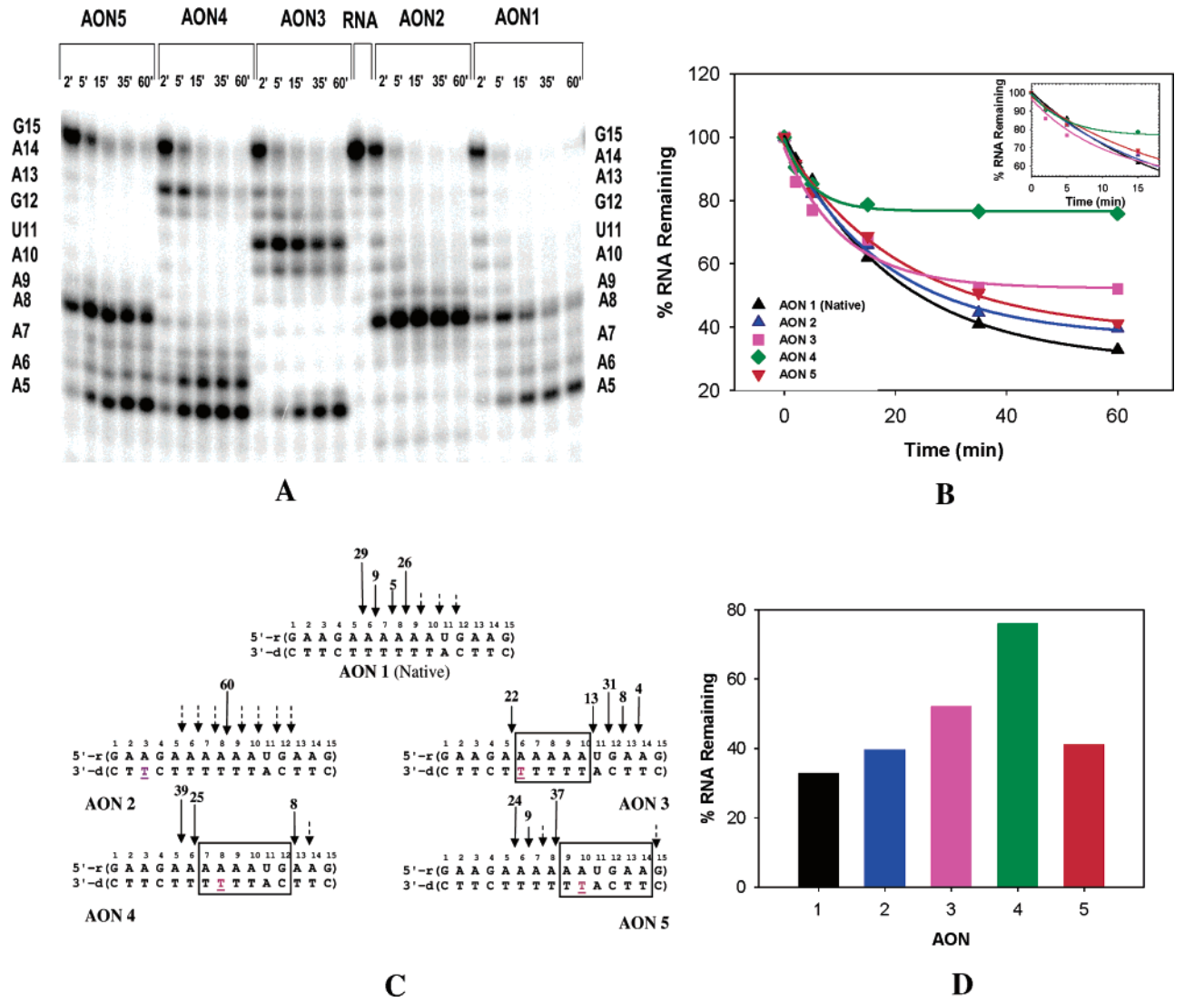

Figure 5. (A) Autoradiograms of 20% denaturing PAGE, showing the cleavage kinetics of 5′-^{32}P-labeled target RNA by *E. coli* RNase H1 in native AON 1/RNA (lane 5) and the aza-ENA-T-modified AONs (2−5)/RNA hybrid duplexes (lanes 1−4) after 2, 5, 15, 35, and 60 min of incubation. Conditions of cleavage reactions: RNA (0.8 μM) and AONs (4 μM) in buffer containing 20 mM Tris-HCl (pH 8.0), 20 mM KCl, 10 mM $MgCl_2$, and 0.1 mM DTT at 21 °C; 0.08 unit of RNase H. Total reaction volume 30 μL. (B) Kinetics of RNase H cleavage. The target RNA remaining is densitometrically evaluated and plotted as a function of time. The inset in the right corner shows the initial cleavage rates for clarity. (C) Pictorial representation of RNase H1 cleavage pattern of AONs 1−5/RNA hybrid duplexes. Vertical arrows show the RNase H cleavage sites, with the relative length of an arrow showing the relative extension of cleavage at that site, and dotted arrows show the partial cleavage at the initial reaction time. The relative percentage of cleavage is indicated above the arrow, which is taken at a 15 min time point from the gel shown above. (D) Quantitative evaluation of the gel picture (shown in the Supporting Information) of the remaining full-length [^{32}P]RNA at 1 h as obtained by the densitometer.

AONs were tested against human serum, which is mainly comprised of 3′-exonucleases (Figure 7). When compared to the native counterpart, which completely degraded after 9 h, AON 3, 4, and 5 (Table 1) were still remaining to a certain extent (8, 15, and 20%, respectively). It is noteworthy that all modified AONs were cleaved by 3′-exonucleases in the blood serum at the phosphodiester, which is one nucleotide before the aza-ENA-T modification site toward the 3′ end, and the residual sequences were found to be stable in human serum for 48 h at 21 °C (Figure S5 in the Supporting Information). This is a surprising result in view of the fact that identical AON sequences with North-constrained oxetane[75] modification are cleaved at the phosphodiester immediately before the modification site under an identical condition. This suggests that the conformational effect of the aza-ENA-T modification in the AON is transmitted toward the 3′ end and recognized by 3′-exonucleases, just as in the RNase H cleavage of the AON/RNA duplex, which recognizes the local RNA/RNA-type duplex structure and leaves a footprint at the 5′ end because of the modulation of the structure of the complementary RNA strand by the North-type constrained aza-ENA-T in the AON strand. The stability studies in human serum with a single LNA[73] nucleotide at the 3′ and 5′ ends showed complete degradation in 24 h at 37 °C, while our residual sequences from the aza-ENA-T modifications were stable over 48 h under our experimental condition (Figure S5 in the Supporting Information). Even though a direct comparison could not be made, these results clearly show that aza-ENA-T modification can certainly give substantial stability in human serum, which is probably more than that of LNA.

(75) Pradeepkumar, P. I.; Amirkhanov, N. V.; Chattopadhyaya, J. *Org. Biomol. Chem.* **2003**, *1*, 81.

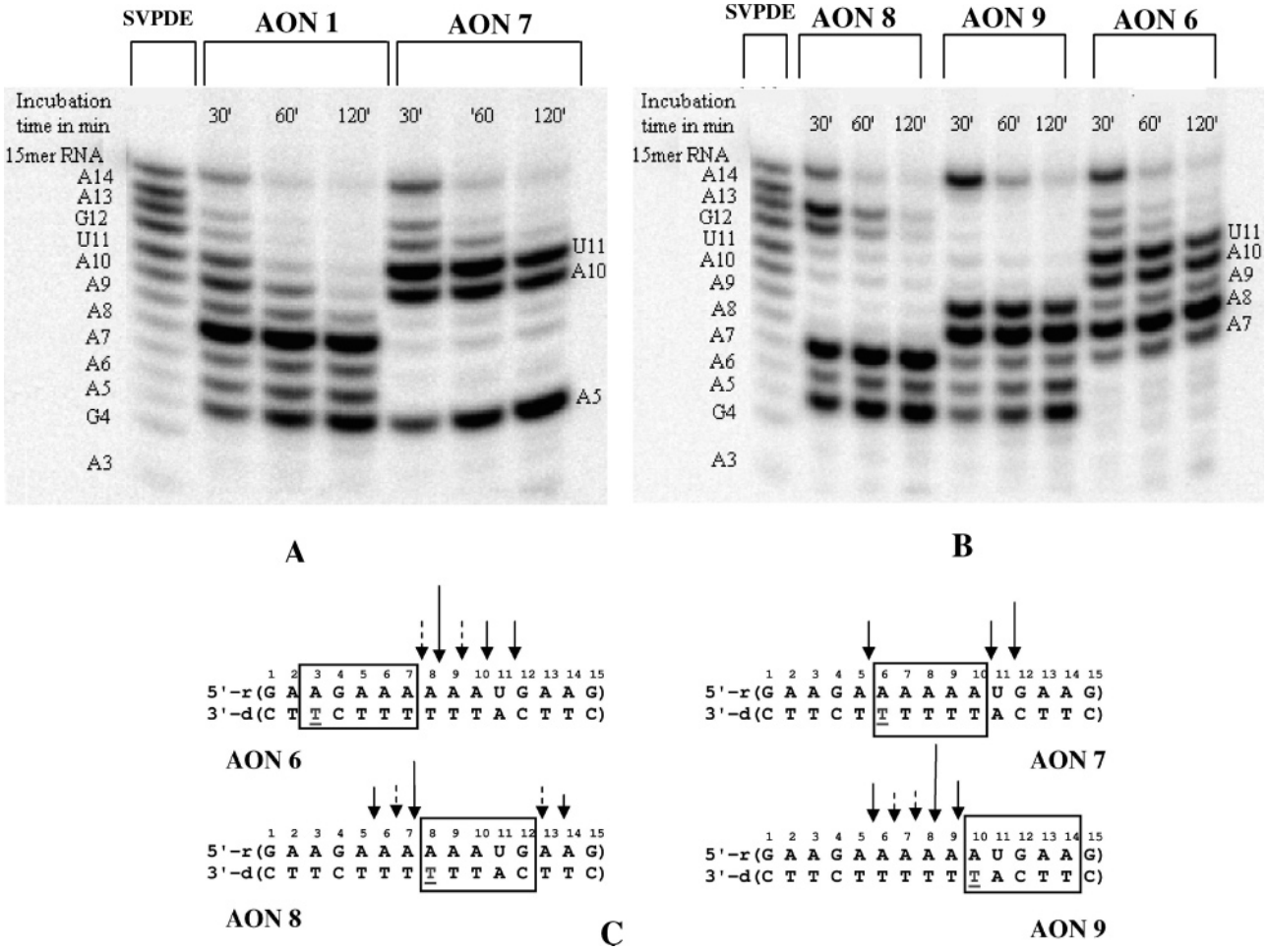

Figure 6. (A and B) are autoradiograms of 20% denaturing PAGE, showing the cleavage kinetics of 5′-^{32}P-labeled target RNA by *E. coli* RNase H1 in native AON 1/RNA and the oxetane-modified AONs (6−9)/RNA hybrid duplexes after 30 min and 1 and 2 h of incubation. Conditions of cleavage reactions: RNA (0.8 μM) and AONs (4 μM) in buffer containing 20 mM Tris-HCl (pH 8.0), 20 mM KCl, 10 mM $MgCl_2$, and 0.1 mM DTT at 21 °C; 0.08 unit of RNase H. Total reaction volume of 30 μL. (C) Pictorial representation of the RNase H1 cleavage pattern of AONs (6−9)/RNA hybrid duplexes. Vertical arrows show the RNase H cleavage sites, with the relative length of an arrow showing the relative extension of cleavage at that site, and dotted arrows show the cleavage at the initial 30 min of the reaction.

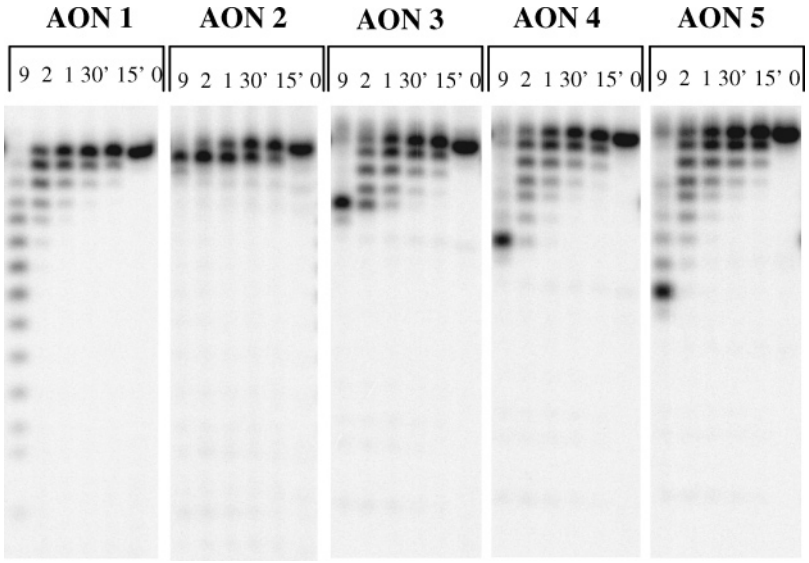

Figure 7. Autoradiograms of 20% denaturing PAGE, showing the degradation pattern of 5′-^{32}P-labeled AONs 1−5 in human serum. Time points are taken after 0, 15, and 30 min and 1, 2, and 9 h of incubation. The percentage of AON remaining after 9 h of incubation: 0% of AON 1, 0% of AON 2, 8% of AON 3, 15% of AON 4, and 20% of AON 5.

9. 3′-Exonuclease Stability Assay [Snake Venom Phosphodiesterase (SVPDE)]. The stability of aza-ENA-T-modified AONs 1−5 toward 3′-exonuclease was investigated using SVPDE over a period of 24 h at 21 °C. Time points were taken

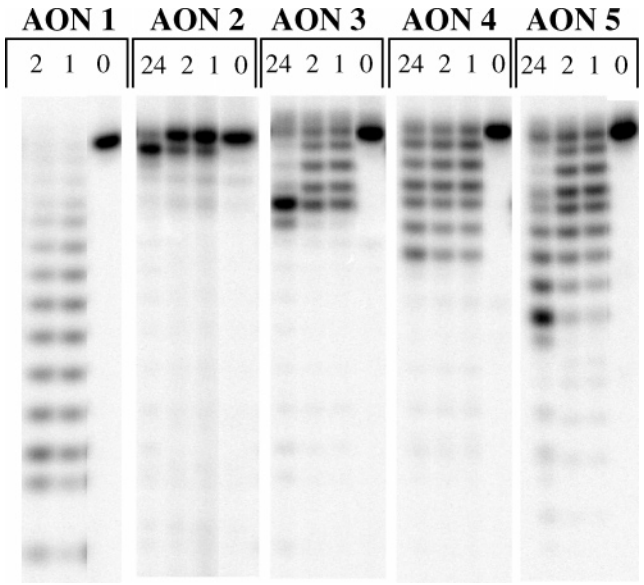

Figure 8. Denaturing PAGE analysis of the SVPDE degradation pattern of 5′-^{32}P-labeled AONs 1−5. Time points are taken after 0, 1, 2, and 24 h of incubation with the enzyme. The percentage of AON remaining after 24 h of incubation: 0% of AON 1, 18% of AON 2, 20% of AON 3, 14% of AON 4, and 10% of AON 5.

at 0, 1, 2, and 24 h to examine the cleavage pattern (Figure 8). The enzyme digestion pattern was similar to that obtained from the digestion with human serum, except the fact that these aza-ENA-T-modified AONs offered resistance to degradation even after 24 h. Note that native AON 1 was completely degraded in 1 h, whereas the full-length AONs 2−5 were 18, 20, 14, and 10% left undegraded, respectively, after 24 h. It is however noteworthy that, similar to the blood serum digestion, all modified AONs were cleaved by SVPDE at the phosphodiester, which is one nucleotide before the aza-ENA-T modification site toward the 3′ end, and the residual sequences were found to be fully stable for 24 h at 21 °C (Figure 8). This is another proof for the future design of aza-ENA-T-modified AONs, where only a single modification at the second position from the 3′ end will offer significant stability toward 3′-exonucleases.

Conclusions

(1) In the cyclization of **11** → **12a** + **12b**, two pure diastereomers were isolated because of the axial and equatorial orientation of the chiral piperidino-NH proton (**12a**, NH_e; **12b**, NH_a) for the first time. The conversion of **12b** to **12a** in pyridine-d_5 is nonreversible ($\Delta G^{\ddagger}$ at 298 K = 23.4 kcal mol^{-1}). In $CDCl_3$, diastereomers **12a** ⇆ **12b** (60:40 by ^{1}H NMR) were however in dynamic equilibrium with $K_c = 0.67$, with the $\Delta G^{\ddagger} = 25.4$ kcal mol^{-1}. (2) The molecular structures of the aza-ENA-T monomer units by high-field ^{1}H NMR and theoretical *ab initio* and MD simulations have shown that the piperidino-fused furanose ring is indeed locked in the typical North-type conformation, with the pseudorotational phase angle (P) and puckering amplitude (ϕ_m) for the *ab initio* optimized geometries (HF, 6-31G**) varying in the ranges $7° < P < 27°$ and $44° < \phi_m < 52°$, respectively. (3) Aza-ENA-T-modified AONs have shown high target affinity to the complementary RNA strand (T_m increase of +2.5 to +4 °C per modification), depending upon the substitution site, compared to the native counterpart, while hybridization with the complementary DNA sequence lead to substantial destabilization of the duplexes (T_m drop of −0.5 to −3 °C per modification). (4) All of the aza-ENA-T-modified AON/RNA hybrid duplexes have been found to be good substrates for the *E. coli* RNase H1. In these AON/RNA hybrids, except for one case (AON 2, Figure 8), a region of 5−6 nucleotides in the RNA strand in the 3′-end direction from the site opposite to the aza-ENA-T modification was found to be insensitive toward RNase H cleavage, presumably owing to the local structural perturbations brought about by the conformational constrain. These cleavage patterns of the aza-ENA-T-modified AON/RNA hybrids are uniquely different from that of the oxetane-modified AONs, which had shown a gap of 5 nucleotide units. (5) All of the aza-ENA-T-modified AONs offered greater protection toward 3′-exonucleases compared to the native sequence (stable for over 48 h in human serum). (6) This study provides valuable information regarding the optimal design of AONs having a completely natural phosphodiester backbone for the therapeutic applications that will not only show high target affinity but also favorable RNase H recruitment as well as high stability toward nucleases *in vivo*.

Experimental Section

Compound C in Scheme 1: [(1*R*,3*R*,4*R*,6*S*)-1-Benzyloxymethyl-6-benzyloxy-5-carbonitrile-3-(thymin-1-yl)-2-oxabicyclo[2.1.1]-hexane]. The nucleoside **11** (2.5 g, 4.1 mmol) was dissolved in 45 mL of dry THF and cooled in an ice bath, and 1 M NaHMDS (8.2 mL) was added dropwise. The reaction was warmed slowly to room temperature and stirred for 3 h under nitrogen, which was then quenched by adding water and extracted with CH_2Cl_2 (3 times). The organic phase was dried over anhydrous $MgSO_4$, filtered, and concentrated under reduced pressure. The crude residue was purified by silica gel column chromatography (0−3% methanol in dichloromethane, v/v), which afforded **C** in Scheme 1 with traces of another diastereomer as shown by NMR (655 mg, 1.4 mmol, 35%). $R_f = 0.40$ [96:4 CH_2Cl_2/CH_3OH (v/v)]. MALDI−TOF m/z: $[M + H]^+$ found, 460.9; calcd, 459.1. ^{1}H NMR (500 MHz, major isomer, $CDCl_3$) δ: 8.93 (s, 1H, NH, thymine), 7.45−7.12 (m, 10H, Bn), 6.92 (q, J = 1.2 Hz, 1H, H6), 5.81 (s, 1H, H6′; H6′ appears as t with a resolution enhancement, W coupling, $J_{H6',H3'}$ = 1.5 H and $J_{H6',H5'}$ = 1.5 Hz), 5.08 (d, $J_{H1',H2'}$ = 2.5 Hz, 1H, H1′), 4.58 (d, J_{gem} = 13.4 Hz, 1H, CH_2Ph), 4.50−4.46 (m, 5H, CH_2Ph, H5′, H5″), 3.96 (dd, $J_{H2',H3'}$ = 7.7, $J_{H3',H6'}$ = 1.5 Hz, 1H, H3′), 3.25 (dd, $J_{H1',H2'}$ = 7.7, $J_{H2',H3'}$ = 2.5 Hz, 1H, H2′), 1.50 (d, J = 1.2 Hz, CH_3, thymine). ^{13}C NMR (125.7 MHz, $CDCl_3$) δ: 163.2 (C4), 159.9 (C4′), 150.2 (C2), 136.6, 135.7, 134.4 (C6), 128.6, 128.5, 128.4, 128.2, 128.0, 127.8, 115.1 (CN), 110.3 (C5), 99.3 (C6′), 73.2 (CH_2Ph), 71.7 (CH_2Ph), 70.7 (C5′), 68.3 (C3′), 63.6 (C1′), 58.8 (C2′), 11.9 (CH_3, thymine). ^{1}H NMR (500 MHz, minor isomer, $CDCl_3$) δ: 7.39−7.15 (m, 10H, Bn), 7.07 (q, J = 1.5 Hz, 1H, H6), 5.09 (d, $J_{H1',H2'}$ = 2.5 Hz, 1H, H1′), 4.65−4.40 (m, 6H, 2×CH_2Ph, H5′, H5″), 4.06 (d, $J_{H2',H3'}$ = 8.2 Hz, 1H, H3′), 3.35 (dd, $J_{H2',H3'}$ = 8.2 Hz, $J_{H1',H2'}$ = 2.5 Hz, 1H, H2′), 1.78 (d, J = 1.5 Hz, CH_3, thymine). ^{13}C NMR (125.7 MHz, $CDCl_3$) δ: 163.4, 160.0, 150.0, 137.0, 136.4, 135.3, 134.6, 128.9−127.6, 117.6, 115.5, 114.8, 112.9, 99.7, 73.8, 71.8, 71.3, 68.1, 64.9, 57.7, 12.2.

3,5-Di-*O*-benzyl-4-*C*-hydroxymethyl-1,2-*O*-isopropylidene-α-D-ribofuranose (2). To a stirred suspension of **1** (12.3 g, 39.5 mmol) in anhydrous acetonitrile (400 mL) at −5 °C was added NaH (1.81 g, 1.15 mmol) in four portions during 1.5 h. Benzyl bromide (5.4 mL, 1.15 mmol) was added dropwise and stirred at room temperature overnight under nitrogen atmosphere. The reaction was quenched with water and extracted with dichloromethane. The organic phase was dried over anhydrous $MgSO_4$ and evaporated under reduced pressure. The crude product was purified by silica gel column chromatography (0−

20% ethyl acetate in cyclohexane, v/v), which afforded **2** (10.6 g, 26.5 mmol, 67%). All analytical data were identical to those previously reported.[21]

3,5-Di-*O*-benzyl-4-*C*-cyanomethyl-1,2-*O*-isopropylidene-α-D-ribofuranose (4). The sugar **2** (10.6 g, 26.5 mmol) was dissolved in an anhydrous dichloromethane/pyridine mixture (250 mL, 3:1, v/v) and cooled in an ice bath. To this solution, triflic anhydride (5.3 mL, 31.8 mmol) was added dropwise and stirred for 3 h under nitrogen atmosphere. The reaction was quenched with cold saturated aqueous $NaHCO_3$ and extracted with dichloromethane. The organic phase was dried over anhydrous $MgSO_4$ and evaporated under reduced pressure followed by co-evaporation with toluene 3 times and dichloromethane 3 times. The crude reaction product was dissolved in 150 mL of dry DMF, and 80 mL of 1 M LiCN in DMF was added and stirred for 3 days at room temperature. The solvent was evaporated, and the residue was dissolved in dichloromethane. Saturated aqueous $NaHCO_3$ was added and extracted with dichloromethane (3 times). The organic phase was dried over anhydrous $MgSO_4$ and evaporated under reduced pressure. The crude product was purified by silica gel column chromatography (0−20% ethylacetate in cyclohexane, v/v), which afforded **4** (6.06 g, 14.8 mmol, 56%). $R_f = 0.61$ [60:40 cyclohexane/ethylacetate (v/v)]. MALDI−TOF *m*/*z*: $[M + H]^+$ found, 410.0; calcd, 409.1. ^{1}H NMR (270 MHz, $CDCl_3$) δ: 7.32−7.2 (m, 10H, benzyl), 5.71 (d, $J_{H1,H2} = 3.71$ Hz, 1H, H1), 4.74 (d, $J_{gem} = 12$ Hz, 1H, CH_2Ph), 4.59−4.52 (m, 4H, H2, CH_2Ph, 2×CH_2Ph), 4.06 (d, $J_{H2,H3} = 4.95$ Hz, 1H, H3), 3.5 (ABq, $J_{gem} = 10.39$ Hz, 2H, H5′, H5″), 3.15 (d, $J_{gem} = 17.07$ Hz, 1H, H6′), 2.86 (d, 1H, H6″), 1.58 (s, 3H, CH_3, isopropyl), 1.32 (s, 3H, CH_3, isopropyl). ^{13}C NMR (67.9 MHz, $CDCl_3$) δ: 137.3, 137, 128.3, 128.2, 127.7, 127.5, 117.0 (CN), 113.4 (q, isopropyl), 103.9 (C1), 83.2 (q, C4), 78.4 (C2), 78 (C3), 73.6 (CH_2Ph), 72.4 (CH_2Ph, C5), 26.5 (CH_3, isopropyl), 25.6 (CH_3, isopropyl), 22.1 (C6).

1-[2-*O*-Acetyl-3,5-di-*O*-benzyl-4-*C*-cyanomethyl-β-D-ribofuranosyl]thymine (6). Triflic acid (0.065 mL, 0.74 mmol) was added dropwise to a stirred solution of **4** (6.06 g, 14.8 mmol) in acetic acid (89 mL) and acetic anhydride (16.7 mL, 177.6 mmol). The solution was stirred for 3 h at room temperature and then poured into a cold $NaHCO_3$ solution. The mixture was extacted with dichloromethane, and the organic phase was dried over anhydrous $MgSO_4$ and evaporated under reduced pressure. The crude product was co-evaporated several times with dry toluene until the product solidifies to give **5** (more than 90% pure by NMR). The crude product was dissolved in 150 mL of anhydrous CH_3CN, and thymine (2.24 g, 17.7 mmol) and *N*,*O*-bis-(trimethylsilyl)acetamide (10.2 mL, 41.4 mmol) were added and stirred at 80 °C for 1 h under a nitrogen atmosphere. The reaction mixture was cooled to room temperature, and TMSOTf (3.48 mL, 19.24 mmol) was added, again warmed to 80 °C, and stirred overnight under a nitrogen atmosphere. The reaction was quenched with saturated aqueous $NaHCO_3$ and extracted with dichloromethane. The organic phase was dried over anhydrous $MgSO_4$, evaporated under reduced pressure, and purified by silica gel column chromatography (0−3% methanol in dichloromethane, v/v) to afford **6** (6.14 g, 11.8 mmol, 80%). $R_f = 0.56$ [96:4 CH_2Cl_2/CH_3OH (v/v)]. MALDI−TOF *m*/*z*: $[M + H]^+$ found, 520.0; calcd, 519.2. ^{1}H NMR (270 MHz, $CDCl_3$) δ: 8.8 (br s, 1H, NH), 7.35−7.24 (m, 11H, benzyl, H6), 6.1 (d, $J_{H1',H2'} = 4.8$ Hz, 1H, H1′), 5.50 (app t, $J = 5.32$ Hz, 1H, H2′), 4.62 (d, $J_{gem} = 11.13$ Hz, CH_2Ph), 4.53−4.44 (m, 4H, H3′, CH_2Ph, 2×CH_2Ph), 3.80 (d, $J_{gem} = 10.14$ Hz, 1H, H5′), 3.63 (d, 1H, H5″), 2.75 (ABq, $J_{gem} = 17.07$ Hz, 2H, H6′, H6″), 2.10 (s, 3H, OAc), 1.60 (s, 3H, CH_3, thymine). ^{13}C NMR (67.9 MHz, $CDCl_3$) δ: 169.7 (CO), 163.3 (C4), 150.1 (C2), 136.6, 135.8 (C6), 128.6, 128.4, 128.1, 128.0, 116.3 (CN), 111.5 (q, C5), 87.9 (C1′), 84.7 (q, C4′), 77.1 (C3′), 74.7 (CH_2Ph), 74.3 (C2′), 73.7 (C5′), 22.2 (C6′), 20.5 (CH_3, OAc), 11.9 (CH_3, thymine).

1-[3,5-Di-*O*-benzyl-4-*C*-cyanomethyl-2-*O*-methanesulfonyl-β-D-ribofuranosyl]thymine (8). Nucleoside **6** (6.14 g, 11.8 mmol) was dissolved in methanol (60 mL), and 18 mL of 1 M sodium methoxide was added and stirred at room temperature for 3 h. The solvent was partially evaporated under reduced pressure and extracted with dichloromethane. The combined organic phase was dried over anhydrous $MgSO_4$ and evaporated to give **7** (more than 90% pure by NMR) as a white solid. The crude product was co-evaporated with dry pyridine 3 times to remove traces of moisture and dissolved in 60 mL of the same solvent. The reaction was cooled in an ice bath, and methanesulfonyl chloride (1.8 mL, 23.6 mmol) was added dropwise and stirred at 0 °C for 6 h. The reaction was quenched with saturated aqueous $NaHCO_3$ and extracted with dichloromethane. The organic phase was dried over anhydrous $MgSO_4$, evaporated under reduced pressure, and co-evaporated 3 times with toluene and 3 times with dichloromethane. The product was purified using silica gel column chromatography (0−3% methanol in dichloromethane, v/v) to afford **8** (6.2 g, 11.2 mmol, 95%). $R_f = 0.41$ [96:4 CH_2Cl_2/CH_3OH (v/v)]. MALDI−TOF *m*/*z*: $[M + H]^+$ found, 556.0; calcd, 555.1. ^{1}H NMR (270 MHz, $CDCl_3$) δ: 10.1 (br s, 1H, NH), 7.46 (s, H6), 7.33−7.2 (m, 10H, benzyl), 6.05 (d, $J_{H1',H2'} = 2.72$ Hz, 1H, H1′), 5.39 (m, 1H, H2′), 4.84 (d, $J_{gem} = 11.38$ Hz, 1H, CH_2Ph), 4.53−4.40 (m, 4H, H3′, CH_2Ph, 2×CH_2Ph), 3.88 (d, $J_{gem} = 10.27$ Hz, 1H, H5′), 3.56 (d, 1H, H5″), 3.15 (s, 3H, OMs), 2.92 (d, $J_{gem} = 17.32$ Hz, 1H, H6′), 2.71 (1H, H6″), 1.45 (s, 3H, CH_3, thymine). ^{13}C NMR (67.9 MHz, $CDCl_3$) δ: 163.7 (C4), 150.5 (C2), 136.3 (C6), 136.2, 135.3, 128.7, 128.4, 128.3, 128.1, 128.0, 116.1 (CN), 111.1 (q, C5), 85.6 (C1′), 84.7 (q, C4′), 79.2 (C2′), 75.3 (C3′), 73.7 (CH_2Ph), 73.4 (CH_2Ph), 70.8 (C5′), 38.6 (OMs), 22.1 (C6′), 11.6 (CH_3, thymine).

2,2′-Anhydro-1[3,5-di-*O*-benzyl-4-*C*-cyanomethyl-β-D-ribofuranosyl]thymine (9). Nucleoside **8** (6.2 g, 11.2 mmol) was dissolved in 70 mL of anhydrous CH_3CN, and DBU (1.75 mL, 11.76 mmol) was added dropwise and stirred at room temperature for 1 h. The reaction was quenched with water and extracted with dichloromethane. The combined organic phase was dried over anhydrous $MgSO_4$ and evaporated under reduced pressure. The crude product was purified by silica gel column chromatography (0−4% methanol in dichloromethane, v/v) to afford **9** (4.7 g, 10.2 mmol, 91%). $R_f = 0.21$ [96:4 CH_2Cl_2/CH_3OH (v/v)]. MALDI−TOF *m*/*z*: $[M + H]^+$ found, 460.0; calcd, 459.1. ^{1}H NMR (270 MHz, $CDCl_3$) δ: 7.35−7.12 (m, 11H, benzyl, H6), 6.25 (br d, $J_{H1',H2'} = 3.8$ Hz, 1H, H1′), 5.32 (br d, 1H, $J_{H2',H1'} = 3.6$ Hz, H2′), 4.77 (d, $J_{gem} = 11.63$ Hz, 1H, CH_2Ph), 4.62 (d, 1H, CH_2Ph), 4.43−4.31 (m, 3H, H3′, 2×CH_2Ph), 3.36 (d, $J_{gem} = 10.02$ Hz, 1H, H5′), 3.23 (d, 1H, H5″), 2.80 (d, $J_{gem} = 16.70$ Hz, 1H, H6′), 2.7 (d, 1H, H6″), 1.96 (s, 3H, CH_3, thymine). ^{13}C NMR (67.9 MHz, $CDCl_3$) δ: 171.9 (C4), 159.0 (C2), 136, 135.4, 129.7 (C6), 128.7, 128.6, 128.4, 128.1, 127.8, 119.4 (q, C5), 116.4 (CN), 89.6 (C1′), 88.1 (q, C4′), 85.7 (C2′), 83.4 (C3′), 73.7 (CH_2Ph), 73.3 (CH_2Ph), 71.1 (C5′), 22.2 (C6′), 13.9 (CH_3, thymine).

1-[3,5-Di-*O*-benzyl-4-*C*-cyanomethyl-β-D-arabinofuranosyl]thymine (10). To a solution of **9** (4.7 g, 10.2 mmol) in 200 mL of acetone, 204 mL of 0.1 M H_2SO_4 was added and refluxed overnight with stirring. The solvent was partially evaporated, and saturated aqueous $NaHCO_3$ was added and extracted with dichloromethane. The organic phase was dried over anhydrous $MgSO_4$ and evaporated under reduced pressure to give **10** quantitatively. $R_f = 0.35$ [96:4 CH_2Cl_2/CH_3OH (v/v)]. MALDI−TOF *m*/*z*: $[M + H]^+$ found, 478.1; calcd, 477.1. ^{1}H NMR (270 MHz, $CDCl_3$) δ: 11.1 (br s, 1H, NH), 7.38−7.23 (m, 11H, benzyl, H6), 6.18 (d, $J_{H1',H2'} = 3.09$ Hz, 1H, H1′), 5.22 (d, $J = 4.45$ Hz, 1H, 2′-OH), 4.89 (m, 1H, H2′), 4.66−4.52 (m, 3H, CH_2Ph, 2×CH_2Ph), 4.41 (d, $J_{gem} = 11.5$ Hz, 1H, CH_2Ph), 4.05 (s, 1H, H3′), 3.80 (ABq, $J_{gem} = 9.5$ Hz, 2H, H5′, H5″), 2.90 (d, $J_{gem} = 16.70$ Hz, 1H, H6′), 2.73 (d, 1H, H6″), 1.62 (s, 3H, CH_3, thymine). ^{13}C NMR (67.9 MHz, $CDCl_3$) δ: 165.9 (C4), 150.3 (C2), 138.7 (C6), 137.1, 136.6, 128.3, 128.1, 127.9, 127.8, 127.5, 117.1 (CN), 107.6 (q, C5), 87.3 (C1′), 84.5 (q, C4′), 83.5 (C3′), 73.5 (CH_2Ph), 72.9 (C2′), 71.9 (CH_2Ph), 70.8 (C5′), 21.6 (C6′), 12.1 (CH_3, thymine).

1-[3,5-Di-*O*-benzyl-4-*C*-cyanomethyl-2-*O*-trifluoromethanesulfonyl-β-D-arabinofuranosyl]thymine (11). Nucleoside **10** (4.8 g, 10.2 mmol) was co-evaporated 3 times with dry pyridine to remove traces of moisture and dissolved in a mixture of anhydrous dichloromethane

(40 mL) and anhydrous pyridine (10 mL). To this solution, DMAP (5 g, 40.8 mmol) was added and cooled in an ice bath, and trifluoromethanesulfonic anhydride was added dropwise and stirred under a nitrogen atmosphere for 2.5 h. The reaction was quenched with cold saturated aqueous $NaHCO_3$ and extracted with dichloromethane. The organic phase was dried over anhydrous $MgSO_4$, evaporated under reduced pressure, and co-evaporated with toluene (3 times) and dichloromethane (3 times). The crude product was purified by silica gel column chromatography (0−2% methanol in dichloromethane, v/v) to afford **11** (5.2 g, 8.5 mmol, 84%). $R_f = 0.58$ [96:4 CH_2Cl_2/CH_3OH (v/v)]. MALDI−TOF *m/z*: $[M + H]^+$ found, 609.99; calcd, 609.1. ^1H NMR (270 MHz, $CDCl_3$) δ: 9.47 (br s, 1H, NH), 7.38−7.20 (m, 10H, benzyl), 7.15 (d, $J_{H6,H-CH_3} = 1.11$ Hz, 1H, H6), 6.33 (d, $J_{H1',H2'} = 3.59$ Hz, 1H, H1′), 5.47 (br d, $J = 2.85$ Hz, 1H, H2′), 4.81 (d, $J_{gem} = 11.63$ Hz, 1H, CH_2Ph), 4.59−4.48 (m, 3H, CH_2Ph, 2×CH_2Ph), 4.42 (s, 1H, H3′), 3.73 (d, $J_{gem} = 9.65$ Hz, 1H, H5′), 3.57 (d, 1H, H5″), 2.90 (d, $J_{gem} = 16.95$ Hz, 1H, H6′), 2.76 (d, 1H, H6″), 1.85 (d, $J_{H6,H-CH_3} = 1.1$ Hz, 3H, CH_3, thymine). ^{13}C NMR (67.9 MHz, $CDCl_3$) δ: 163.2 (C4), 149.8 (C2), 136.4 (C6), 135.1, 134.9, 128.6, 128.5, 128.2, 128.1, 127.6, 118 (q, $J = 320.2$ Hz, CF_3), 116.3 (CN), 111.2 (C5), 85.4 (C2′), 83.9 (C1′), 83.6 (C4′), 82.2 (C3′), 73.66 (CH_2Ph), 73.60 (CH_2Ph), 70.7 (C5′), 21.7 (C6′), 12.2 (CH_3, thymine).

(1*R*,5*R*,7*R*,8*S*)-5-Benzyloxymethyl-8-benzyloxy-7-(thymin-1-yl)-2-aza-6-oxabicyclo[3.2.1]octane (12a and 12b). To a solution of **11** (5.2 g, 8.5 mmol) in 120 mL of dry THF, $NaBH_4$ (965 mg, 25.5 mmol) was added. To this suspension, trifluoroacetic acid (1.3 mL, 17 mmol) was added dropwise over a period of 30 min under a nitrogen atmosphere and stirred overnight at room temperature. After complete conversion, excess $NaBH_4$ was hydrolyzed carefully with water, stirred at room temperature for 2 h, and extracted with dichloromethane. Note that if the reaction is worked up after 30 min after hydrolyzing, $NaBH_4$ gives a substantial amount of minor isomer, indicating that this isomer is the kinetic product that converts to the major isomer in the presence of NaOH formed during hydrolyzing $NaBH_4$. The organic phase was dried over anhydrous $MgSO_4$ and evaporated under reduced pressure. Purification by silica gel column chromatography (0−6% methanol in dichloromethane, v/v) afforded **12a** (1.6 g, 3.4 mmol, 40%) along with the other diasteriomer **12b** as a minor product (190 mg, 0.4 mmol, 5%). (Major diastereomer **12a**). $R_f = 0.42$ [90:10 CH_2Cl_2/CH_3OH (v/v)]. MALDI−TOF *m/z*: $[M + H]^+$ found, 464.1; calcd, 463.2. ^1H NMR (500 MHz, $CDCl_3$) δ: 7.97 (q, J= 1.3 Hz, H6, thymine), 7.37−7.24 (m, 10H, benzyl), 5.94 (s, 1H, H1′), 4.68 (d, $J = 11.8$ Hz, 1H, CH_2Ph), 4.57 (d, $J = 11.5$ Hz, 1H, CH_2Ph), 4.53 (d, $J = 11.8$ Hz, 1H, CH_2Ph), 4.51 (d, $J = 11.5$ Hz, 1H, CH_2Ph), 3.98 (d, $J = 3.9$ Hz, 1H, H3′), 3.71 (d, $J = 10.8$ Hz, 1H, H5′), 3.58 (d, $J = 10.8$ Hz, 1H, H5″), 3.52 (d, $J = 3.9$ Hz, 1H, H2′), 3.13 (ddd, $J = 13.3$, 11.6, 4.9 Hz, 1H, $H7_a'$), 3.02 (dd, $J = 13.3$, 6.5 Hz, 1H, $H7_e'$), 2.03 (ddd, $J = 13.1$, 11.6, 6.7 Hz, 1H, $H6_a'$), 1.43 (d, $J = 1.3$ Hz, 1H, CH_3, thymine), 1.31 (dd, $J = 13.1$, 4.8 Hz, 1H, $H6_e'$). ^{13}C NMR (125.7 MHz, $CDCl_3$) δ: 163.9 (C4), 150.0 (C2), 137.4, 137.2, 135.7 (C6), 128.5, 128.3, 128.1, 128.0, 127.8, 109.4 (C5), 87.0 (C1′), 84.4 (C4′), 73.4 (CH_2Ph), 71.8 (CH_2Ph), 71.7 (C3′), 70.3 (C5′), 59.1 (C2′), 38.4 (C7′), 27.5 (C6′), 11.7 (CH_3, thymine).

(Minor diastereomer **12b**). $R_f = 0.71$ [92:8 CH_2Cl_2/CH_3OH (v/v)]. MALDI−TOF *m/z*: $[M + H]^+$ found, 464.0; calcd, 463.2. ^1H NMR (600 MHz, $CDCl_3$) δ: 7.95 (s, 1H, NH, thymine), 7.77 (q, $J = 1.2$ Hz, 1H, H6, thymine), 7.44−7.24 (m, 10 H, Bn), 6.28 (s, 1H, H1′), 4.64 (d, $J = 11.6$ Hz, 1H, CH_2Ph), 4.58 (d, $J = 11.5$ Hz, 1H, CH_2Ph), 4.56 (d, $J = 11.6$ Hz, 1H, CH_2Ph), 4.53 (dd, $J = 11.92$, 3.91 Hz, 1H, NH), 4.50 (d, $J = 11.5$ Hz, 1H, CH_2Ph), 4.33 (d, $J = 4.1$ Hz, 1H, H3′), 3.73 (d, $J = 11.0$ Hz, 1H, H5′), 3.58 (d, $J = 4.1$ Hz, 1H, H2′), 3.52 (d, $J = 11.0$ Hz, 1H, H5″), 3.26 (ddd, $J = 14.2$, 6.4, 3.9 Hz, 1H, $H7_e'$), 2.98 (dtd, $J = 14.2$, 11.9, 11.9, 5.2 Hz, 1H, $H7_a'$), 2.04 (ddd, $J = 13.4$, 11.9, 6.4 Hz, 1H, $H6_a'$), 1.53 (dd, $J = 13.4$, 5.2 Hz, 1H, $H6_e'$), 1.50 (d, $J = 1.2$ Hz, CH_3, thymine). ^{13}C NMR (125.7 MHz, $CDCl_3$) δ: 163.5 (C4), 149.1 (C2), 136.8, 136.0, 135.6 (C6), 128.6, 128.3, 128.2, 128.0, 127.9, 110.3 (C5), 82.6 (C1′), 82.5 (C4′), 73.68 (CH_2Ph), 73.64 (CH_2Ph), 72.0 (C3′), 69.5 (C5′), 64.2 (C2′), 45.9 (C7′), 26.8 (C6′), 11.9 (CH_3, thymine).

(1*R*,5*R*,7*R*,8*S*)-8-Hydroxy-5-hydroxymethyl-7-(thymin-1-yl)-2-aza-6-oxabicyclo[3.2.1]octane (13). Nucleoside **12a**/**12b** (1.6 g, 3.4 mmol) was dissolved in 15 mL of methanol, and 20% $Pd(OH)_2$ on charcoal (615 mg) was added, followed by ammonium formate (2.5 g, 40 mmol), and refluxed for 12 h. The catalyst was filtered off through a celite bed, and the filtrate evaporated under reduced pressure and co-evaporated with dichloromethane to remove traces of methanol. The crude material was dissolved in 20 mL of anhydrous dichloromethane and cooled to −78 °C, and 1 M BCl_3 (27 mL) was added and stirred under nitrogen atmosphere for 3 h. The reaction was quenched by adding methanol, and volatile materials were removed under reduced pressure to give **13**, which was purified for characterization using silica gel column chromatography (0−20% methanol in dichloromethane, v/v) to give **13** in 60% yield. $R_f = 0.18$ [80:20 CH_2Cl_2/CH_3OH (v/v)]. MALDI−TOF *m/z*: $[M + H]^+$ found, 284.2; calcd, 284.1. ^1H NMR (600 MHz, DMSO-d_6) δ: 11.30 [s, 1H, NH (thymine)], 8.27 (s, 1H, H6), 5.84 (s, 1H, H1′), 5.39 [t, $J = 5.0$, 5.0 Hz, 1H, OH(5′)], 5.16 [br, 1H, OH(3′)], 3.99 (dd, $J = 3.9$, 4.6 Hz, 1H, H3′), 3.57 (dd, $J = 12.2$, 5.2 Hz, 1H, H5′), 3.50 (dd, $J = 12.2$, 5.2 Hz, 1H, H5″), 3.25 (d, $J = 3.19$ Hz, 1H, H2′), 2.95 (dt, $J = 12.8$, 13.0, 4.8 Hz, 1H, $H7_a'$), 2.87 (dd, $J = 12.8$, 6.6 Hz, 1H, $H7_e'$), 1.78 (dt, $J = 12.9$, 13.0, 6.8 Hz, 1H, $H6_a'$), 1.78 (s, 3H, CH_3, thymine), 1.17 (dd, $J = 12.9$, 4.6 Hz, 1H, $H6_e'$). ^{13}C NMR (600 MHz, DMSO-d_6) δ: 164.9 (C4), 151.0 (C2), 137.0 (C6), 108.5 (C5), 86.3 (C4′), 86.2 (C1′), 64.5 (C3′), 62.3 (C5′), 62.0 (C2′), 38.9 (C7′), 27.2 (C6′), 13.3 (CH_3, thymine).

(1*R*,5*R*,7*R*,8*S*)-5-Benzyloxymethyl-8-benzyloxy-2-phenoxyacetyl-7-(thymin-1-yl)-2-aza-6-oxabicyclo[3.2.1]octane (14). To a solution of **12a** (1.6 g, 3.4 mmol) in pyridine was added phenoxyacetyl chloride (0.6 mL, 4.4 mmol), which was added dropwise and stirred under a nitrogen atmosphere for 2 h. The reaction was quenched with cold saturated aqueous $NaHCO_3$ and extracted with dichloromethane. The organic phase was dried over anhydrous $MgSO_4$, evaporated under reduced pressure, and co-evaporated with toluene (3 times) and dichloromethane (3 times). The crude product was purified by silica gel column chromatography (0−3% methanol in dichloromethane, v/v) to afford **14** (note that **12b** reacted very slowly because it converted to **12a** first and then to **14** in 24 h) (1.4 g, 2.4 mmol, 70%). $R_f = 0.35$ [96:4 CH_2Cl_2/CH_3OH (v/v)]. MALDI−TOF *m/z*: $[M + H]^+$ found, 598.2; calcd, 597.2. ^{13}C NMR (67.9 MHz, $CDCl_3$) δ: 168.6, 166.8, 163.6, 163.5, 157.9, 157.6, 150.0, 149.5, 137.0, 136.9, 135.1, 135.0, 129.5, 129.4, 128.5, 128.3, 128.2, 128.1, 128.0, 127.9, 127.7, 127.4, 121.6, 121.4, 114.6, 114.5, 110.0, 109.8, 87.1, 85.9, 84.7, 84.6, 73.5, 73.4, 72.5, 72.4, 72.5, 72.4, 71.0, 69.6, 69.4, 67.7, 59.5, 55.8, 53.3, 39.1, 36.6, 27.0, 25.6, 11.7.

(1*R*,5*R*,7*R*,8*S*)-8-Hydroxy-5-hydroxymethyl-2-phenoxyacetyl-7-(thymin-1-yl)-2-aza-6-oxabicyclo[3.2.1]octane (15). Nucleoside **14** (1.4 g, 2.4 mmol) was dissolved in 15 mL of methanol, and 20% $Pd(OH)_2$ on charcoal (430 mg) was added, followed by ammonium formate (1.81 g, 28.8 mmol), and refluxed for 12 h. The catalyst was filtered off through a celite bed, and the filtrate evaporated under reduced pressure and co-evaporated with dichloromethane to remove traces of methanol. The crude material was dissolved in 25 mL of anhydrous dichloromethane and cooled to −78 °C, and 1 M BCl_3 (19 mL) was added and stirred under a nitrogen atmosphere for 3 h. Solvent and volatile materials were removed under reduced pressure and co-evaporated with methanol. The residue was purified by silica gel column chromatography (0−4% methanol in dichloromethane, v/v) to give **15** (750 mg, 1.8 mmol, 75%). $R_f = 0.38$ [90:10 CH_2Cl_2/CH_3OH (v/v)]. MALDI−TOF *m/z*: $[M + H]^+$ found, 418.2; calcd, 417.1. ^{13}C NMR (67.9 MHz, CD_3OD) δ: 170.7, 166.9, 159.8, 152.4, 137.9, 137.7, 130.7, 130.6, 122.7, 122.5, 116.2, 116.0, 110.6, 87.8, 87.5, 87.3, 67.9, 66.9, 65.7, 65.4, 63.1, 62.9, 60.4, 37.8, 27.2, 26.5, 12.9.

(1*R*,5*R*,7*R*,8*S*)-5-(4,4′-Dimethoxytrityloxymethyl)-8-hydroxy-2-phenoxyacetyl-7-(thymin-1-yl)-2-aza-6-oxabicyclo[3.2.1]octane (16).

Nucleoside **15** (750 mg, 1.8 mmol) was co-evaporated with anhydrous pyridine to remove traces of water and dissolved in 15 mL of the same solvent, and 4,4′-dimethoxytrityl chloride was added and stirred at room temperature for 7 h. The reaction was quenched using cold saturated aqueous $NaHCO_3$ and extracted with dichloromethane. The organic phase was dried over anhydrous $MgSO_4$, evaporated under reduced pressure, and co-evaporated with toluene (2 times) to remove pyridine partially. The crude product was purified by silica gel column chromatography [0−3% methanol in dichloromethane (v/v), containing 1% pyridine] to afford **16** (1.16 g, 1.6 mmol, 90%). $R_f = 0.30$ [96:4 CH_2Cl_2/CH_3OH (v/v)]. MALDI−TOF *m*/*z*: $[M + H]^+$ found, 720.1; calcd, 719.2. ^{13}C NMR (67.9 MHz, $CDCl_3$ plus DABCO) δ: 168.4, 163.6, 158.6, 157.1, 150.0, 144.1, 135.2, 135.0, 134.6, 129.9, 129.7, 129.5, 128.9, 128.0, 127.7, 127.0, 121.9, 121.6, 114.6, 114.4, 113.2, 110.5, 86.6, 86.0, 67.4, 65.3, 62.2, 62.2, 55.1, 46.7, 36.4, 25.6, 11.9.

(1*R*,5*R*,7*R*,8*S*)-8-(2-(Cyanoethoxy(diisopropylamino)-phosphinoxy)-5-(4,4′-dimethoxytrityloxymethyl)-2-phenoxyacetyl-7-(thymin-1-yl)-2-aza-6-oxabicyclo[3.2.1]octane (17). Compound **16** (1.16 g, 1.6 mmol) was dissolved in 15 mL of dry THF, and diisopropylethylamine (1.4 mL, 8 mmol) was added at 0 °C followed by 2-cyanoethyl-*N*,*N*-diisopropylphosphoramidochloridite (0.71 mL, 3.2 mmol). After 30 min, the reaction was warmed to room temperature and stirred overnight. MeOH (0.5 mL) was added, and stirring was continued for 5 min; thereafter, saturated aqueous $NaHCO_3$ was added and extracted with freshly distilled CH_2Cl_2 (3 times). The organic phase was dried over $MgSO_4$, filtered, and concentrated under reduced pressure. The crude residue was purified by silica gel column chromatography (40−70% CH_2Cl_2 in cyclohexane containing 1% Et_3N), which afforded **17** (1.26 g, 1.37 mmol, 86%) as a mixture of four isomers. $R_f = 0.40$ [96:4 CH_2Cl_2/CH_3OH (v/v)]. MALDI−TOF *m*/*z*: $[M + H]^+$ found, 920.2; calcd, 919.3. ^{31}P NMR (67.9 MHz, $CDCl_3$) δ: 150.7, 150.3, 149.2, 148.1.

(1*R*,5*R*,7*R*,8*S*)-8-Hydroxy-5-hydroxymethyl-2-trifluoroacetyl-7-(thymin-1-yl)-2-aza-6-oxabicyclo[3.2.1]octane (18). The nucleoside **12a** (1.6 g, 3.4 mmol) was deprotected as it was done for **13**, and the crude material was dissolved in methanol (20 mL). DMAP (415 mg, 3.4mmol) and ethyl trifluoroacetate (4 mL, 34 mmol) were added and stirred at room temperature overnight. The solvent was removed under reduced pressure and purified by silica gel column chromatography (0−6% methanol in dichloromethane, v/v) to give **18** (580 mg, 1.5 mmol, 45%). $R_f = 0.43$ [90:10 CH_2Cl_2/CH_3OH (v/v)]. MALDI−TOF *m*/*z*: $[M + H]^+$ found, 380.1; calcd, 379.0. ^{13}C NMR (67.9 MHz, CD_3OD) δ: 166.8, 152.1, 138.4, 137.7, 110.8, 110.7, 87.3, 87.2, 86.8, 65.5, 65.2, 62.6, 62.5, 61.8, 41.5, 39.9, 39.0, 27.4, 26.7, 12.9.

(1*R*,5*R*,7*R*,8*S*)-5-(4,4′-Dimethoxytrityloxymethyl)-8-hydroxy-2-trifluoroacetyl-7-(thymin-1-yl)-2-aza-6-oxabicyclo[3.2.1]octane (19). Nucleoside **18** (580 mg, 1.5 mmol) was co-evaporated with anhydrous pyridine to remove traces of water and dissolved in 15 mL of the same solvent, and 4,4′-dimethoxytrityl chloride was added and stirred at room temperature overnight. The reaction was quenched using cold saturated aqueous $NaHCO_3$ and extracted with dichloromethane. The organic phase was dried over anhydrous $MgSO_4$, evaporated under reduced pressure, and co-evaporated with toluene (2 times) to remove pyridine partially. The crude product was purified by silica gel column chromatography [0−3% methanol in dichloromethane (v/v), containing 1% pyridine] to afford **19** (827 mg, 1.2 mmol, 81%). $R_f = 0.31$ [96:4 CH_2Cl_2/CH_3OH (v/v)]. MALDI−TOF *m*/*z*: $[M + Na]^+$ found, 704.2; calcd, 681.2. ^{13}C NMR (67.9 MHz, $CDCl_3$ plus DABCO) δ: 164.02, 163.5, 158.6, 150.0, 149.7, 144.0, 143.9, 134.5, 129.9, 127.9, 127.2, 127.0, 113.3, 110.6, 86.7, 85.4, 85.3, 65.8, 65.4, 63.0, 62.9, 60.1, 55.1, 46.0, 40.1, 37.3, 29.5, 27.0, 26.1, 11.9, 11.8.

(1*R*,5*R*,7*R*,8*S*)-8-(2-(Cyanoethoxy(diisopropylamino)-phosphinoxy)-5-(4,4′-dimethoxy-trityloxymethyl)-2-trifluoroacetyl-7-(thymin-1-yl)-2-aza-6-oxabicyclo[3.2.1]octane (20). Compound **19** (827 mg, 1.2 mmol) was dissolved in 12 mL of dry THF, and diisopropylethylamine (1.05 mL, 6 mmol) was added at 0 °C followed by 2-cyanoethyl-*N*,*N*-diisopropylphosphoramidochloridite (0.53 mL, 2.4 mmol). After 30 min, the reaction was warmed to room temperature and stirred overnight. MeOH (0.5 mL) was added, and stirring was continued for 5 min; thereafter, saturated aqueous $NaHCO_3$ was added and extracted with freshly distilled CH_2Cl_2 (3 times). The organic phase was dried over anhydrous $MgSO_4$, filtered, and concentrated under reduced pressure. The crude residue was purified by silica gel column chromatography (40−100% CH_2Cl_2 in cyclohexane containing 1% Et_3N), which afforded **20** (645 mg, 0.73 mmol, 61%) as a mixture of four isomers. $R_f = 0.44$ [96:4 CH_2Cl_2/CH_3OH (v/v)]. MALDI−TOF *m*/*z*: $[M + H]^+$ found, 882.2; calcd, 881.3. ^{31}P NMR (109.4 MHz, $CDCl_3$) δ: 150.1, 149.9, 149.8, 149.2.

Acknowledgment. Generous financial support from the Swedish Natural Science Research Council (Vetenskapsrådet), the Swedish Foundation for Strategic Research (Stiftelsen för Strategisk Forskning), and the EU-FP6-funded RIGHT project (project number LSHB-CT-2004-005276) is gratefully acknowledged.

Supporting Information Available: ^{13}C NMR spectra of compounds **4**, **6**−**11**, **14**−**16**, **18**, and **19**; ^{31}P NMR spectra of compounds **17** and **20**; ^{13}C, 1D NOE, HSQC, HMBC NMR spectra of compound **D** (Scheme 1); ^{13}C, HSQC, HMBC, and DQF-COSY NMR spectra of compounds **12a**, **12b**, and **13**; RNase H digestion profile of AONs at 0.08 unit enzyme concentration; denaturing PAGE picture in human serum, tables of ^1H and ^{13}C chemical shifts, and coupling constants of compounds **12a**, **12b**, and **13**; introduction, discussions on assignment, stereochemistry,$^3J_{HH}$ simulation, and NOE studies of **12a**, **12b**, and **13**; analysis of CD of AON/RNA and AON/DNA duplexes; cleavage rates of the AON/RNA duplexes by RNase H; experimental methods and details of theoretical calculations; generalized Karplus parametrization; and details of pK_a determination of 2′-amino-LNA-T and aza-ENA-T. This material is available free of charge via the Internet at http://pubs.acs.org.

JA0634977